POLITECNICO DI TORINO

Nanotechnologies for ICTs
A.a. 2023/2024
Master degree thesis

Patterning conductive tracks within hydrogel matrices for soft bioelectronics devices

Veronica NAVELLO

Supervisor:
Lorenzo LUCHERINI
Advisor:
Prof. Esther AMSTAD

Relator:
Prof. Matteo COCUZZA

SOFT MATERIALS LABORATORY

“Insert catchphrase that

will make this work sound insightful”

-The Reader-

Table of contents

5. Results and discussion

6. Conclusions and outlook

7. Acknowledgements

8. References

Abbreviations

PEG	Poly-ethylene glycol
PVA	Poly-vinyl alcohol
PVP	Poly-vinyl pyrrolidone
LCST	Lower critical solution temperature
UPST	Upper critical solution temperature
PEDOT	Poly-(3,4-ethylene-dioxythiophene)
PPy	Polypyrrole
PANI	Polyaniline
P-AA	Polymerized - Acrylic acid
P-AM	Polymerized - Acrylamide
P-DMAPS	Polymerized - [2-(Methacryloyloxy)ethyl]dimethyl-(3-sulfopropyl)ammonium hydroxide
P-AMPS	Polymerized - 2-Acrylamido-2-methyl-1-propanesulfonic acid
UV	Ultraviolet
MBAA	Methylene bisacrylamide
PI	2-Hydroxy-2-methylpropiophenone
UTM	Universal testing machine
3D	3-dimension
PBS	Phosphate-buffered saline
2D	2-dimension
Micro-CT	Micro-computed tomography
CDD	Charged Coupled Device

LP	Laser Power
SS	Scan Speed
I-V	Current Vs Voltage
PVK	Polyvinylcarbazole

Equation table

Quantity	Equation	Number
Young's modulus	$E = \frac{\sigma}{\epsilon}$	(1)
Stress and Strain	$\varepsilon = \frac{\Delta L}{L_0}, \ \sigma = \frac{F}{A}$	(2)
Swelling ratio	$Q = \frac{Q_s - Q_i}{Q_i}$	(3)
Crosslinker mass	$m_{MBAA=} \frac{m_{monomer} \times M_{w\,MBAA} \times mol\% \times 1000}{M_{w\,monomer}}$	(4)
Dose	$D = \frac{(Pp)^2}{\nu}$	(5)
Resistivity and conductivity	$\rho = \frac{R \times A}{L}, \ \sigma = \frac{1}{\rho}$	(6)
Resonance frequency	$f_{res} = \frac{1}{2\pi\sqrt{LC}}$	(7)

Abstract (English)

Hydrogels are biocompatible polymer-based materials widely used in biomedicine thanks to their mechanical affinity with soft tissues. Besides their characteristics make them ideal candidates to substitute metals and semiconductor devices for bioelectronics applications, the lack of electrical conductivity represents a huge drawback limiting the possibility of functionalizing hydrogels. In this thesis, we introduce a method to exploit electrical conductivity in hydrogels through direct laser writing. Through the two-photon absorption process, we are able to achieve the photoreduction of silver ions into silver nanoparticles and obtain highly localized conductive structures embedded inside the gel matrix. We demonstrate the conductor-like behavior of the written structures and the stability of the silver particles stored into a wet environment, defining the writing parameters to obtain a reproducible and reliable process. In this way we can avoid further processing of the substrates after the direct laser writing and ensure electrical conductivity without compromising the mechanical properties of the hydrogel.

Keywords: *hydrogels, conductivity, photoreduction, functionalization.*

Abstract (Italian)

Gli idrogeli sono materiali biocompatibili a base di polimeri, ampiamente utilizzati in biomedicina grazie alla loro affinità meccanica con i tessuti molli. Oltre alle loro caratteristiche che li rendono candidati ideali per sostituire i metalli e i semiconduttori nelle applicazioni di bioelettronica, la mancanza di conducibilità elettrica rappresenta un enorme svantaggio che limita la possibilità di funzionalizzare gli idrogeli. In questa tesi, introduciamo un metodo per sfruttare la conduttività elettrica negli idrogeli attraverso la scrittura diretta con laser. Attraverso il processo di assorbimento a due fotoni, siamo in grado di ottenere la foto-riduzione degli ioni d'argento in nanoparticelle d'argento e di ottenere strutture conduttive altamente localizzate, incorporate nella matrice del

gel. Dimostriamo il comportamento conduttivo delle strutture scritte e la stabilità delle particelle d'argento conservate in ambiente acquoso, definendo i parametri di scrittura per ottenere un processo riproducibile e affidabile. In questo modo possiamo evitare ulteriori lavorazioni dei substrati dopo la scrittura diretta con laser e garantire la conduttività elettrica senza compromettere le proprietà meccaniche dell'idrogelo.

Parole chiave: *idrogeli, conduttività, foto-riduzione, funzionalizzazione.*

Abstract (French)

Les hydrogels sont des matériaux biocompatibles à base de polymères, largement utilisés en biomédecine grâce à leur affinité mécanique avec les tissus mous. Bien que leurs caractéristiques en fassent des candidats idéaux pour remplacer les métaux et les semi-conducteurs dans les applications bioélectroniques, l'absence de conductivité électrique représente un énorme inconvénient qui limite la possibilité de fonctionnaliser les hydrogels. Dans cette thèse, nous présentons une méthode permettant d'exploiter la conductivité électrique des hydrogels par écriture laser directe. Grâce au processus d'absorption à deux photons, nous sommes en mesure de réaliser la photoréduction des ions d'argent en nanoparticules d'argent et d'obtenir des structures conductrices très localisées, intégrées dans la matrice du gel. Nous démontrons le comportement conducteur des structures écrites et la stabilité des particules d'argent stockées dans un environnement humide, en définissant les paramètres d'écriture pour obtenir un processus reproductible et fiable. De cette manière, nous pouvons éviter un traitement supplémentaire des substrats après l'écriture directe au laser et garantir la conductivité électrique sans compromettre les propriétés mécaniques de l'hydrogel.

Mots clés: *hydrogels, conductivité, photoréduction, fonctionnalisation.*

1. Preface

1.1 Nature as the base of science

Nature has always been an inspiration for humankind throughout history. Men started to learn from it since a very early age, when nature was at once a loving mother and a cruel enemy, and they had to continuously evolve and adapt their lifestyle to survive in a welcoming but still hostile environment. With time, humans began taking what the planet offered and reusing it to their own advantage to make life more comfortable by means of what, later in time, would have been called technology. Starting from this basic evolution process, society evolved and developed to become the highly advanced machine we are part of nowadays. Besides the evident dissimilarities between the ancient world and the modern one, it can be stated that there is still a constant which hasn't changed throughout centuries, that is nature has anyways remained the core from which man can absorb the most different kinds of knowledge and get the inspiration to create even the most advanced of the technological tools.

This influence can be seen in architecture, where bees' honeycombs are an example of optimal space management, as the hexagonal shape of the internal cells allows to get maximum area coverage while minimizing the material usage, in a perfect combo of both aesthetic and functionality. Not only modern works of art but also famous historical scientists make their appearance in the nature-encouraged inventors list, such as Leonardo Da Vinci, who tried to fulfill his dream of flying above Florence by studying the structure of bird wings and building, based on their morphology, what he had called the "Ornitottero", which can be defined as the first attempt of a flying machine whose weight was higher than air, as are today the common airplanes[1]. So many of the comforts we are used to during our everyday life have somehow their roots in wildlife and, exactly as an apple is said to have inspired Newton's gravitational theory, of course the world of material science comes from nature. We ourselves are an Earth-made product, but yet we are not perfect, so science also in this case has tried to find a way to fix where something was broken, to replace what didn't

(a) (b)

Figure 1.1: bee honeycomb (a), hexagonal floor (b)

(a) (b)

Figure 1.2: flying bird (a), Ornitottero (b)

work anymore, or to sense and predict what could go wrong. Trying to solve this consistent problem, researchers have once more tried to imitate nature by using what nature itself provided to mankind and they developed a material able to follow the rules of human anatomy, adapting to the wide range of performances required by the variety of tissues composing our living host and surviving contemporarily inside the insidious environment represented by our body.
Hydrogels are indeed one of the most promising materials that could cover the role of substituting human tissues and represent a great candidate for other applications in the sensing domain, where direct contact with the body, i.e. skin or internal matter, is required. The current machines make use of materials such as metals, silicon, or plastics to interact with the human environment, but their properties are intrinsically far from the soft and wet nature of the tissues, therefore hydrogels made their entrance in the engineered bio-materials thanks to their biocompatibility and tunable properties, trying to help solve the more and more investigated problem of interfacing humans and machines in a long-term, body-friendly and efficient way[2].

2. Introduction

2.1 Hydrogels application and limits

The human body is composed of a variety of tissues and organs with highly dissimilar properties, but a common characteristic can be found in their great amount of water content that can range between 70% and 90%, if we exclude blood and bones where a consistent lower quantity is present (see *Figure 2.1).* Being water the base of most biological processes, the use of dry materials such as silicon, plastics, and metals, is logically a non-optimal choice when it comes to replace or interface with soft biological tissues and the outcome is that implants are likely to cause a foreign body reaction from the immune system, that ends up in compromised performances of the device itself and can endanger the patient. This barrier can be outreached by hydrogels, which have a much higher affinity with tissues, as their network is composed of hydrophilic polymers that allow these materials to retain a large amount of water (>70%), making them the ideal candidates for biomedical applications[3]. Moreover, hydrogels can be engineered to fulfill the range of stiffness required by the different tissues which is typically around 1 Pa to 1 MPa, unlike the previously mentioned materials that are more rigid and give less freedom to tune the elastic properties. The trade-off between mechanical properties and water content

becomes then a crucial point for the making of hydrogels that can efficiently work in a water-based environment. Thanks to those characteristics, hydrogels are being chosen as material in many applications, starting from tissue engineering where the biocompatibility and porosity help the cells to adhere better and to get a sufficient amount of nutrients that allow them to grow[4]. Drug delivery is another application made possible by the porosity of the material because molecules are able to diffuse within the pores present in the matrix and allow to have a controlled release of the drug, depending on the network size and arrangement. Taking advantage instead of the flexibility and softness of the substrates, hydrogels are also used to make strain sensors that can be employed to detect motion or pressure, finding their relevance in fields such as soft robotics and health monitoring. A lot of wearable applications, mostly epidermal ones, are also taking advantage of the biocompatibility and softness to reduce the skin-electrode interfacial impedance, by using hydrogels as a coating that can help the rigid metal electrodes to have better adhesion with the epidermal tissue and maintain a good hydration degree. Despite the remarkable properties of hydrogels, these materials still have an important limitation that narrows the range of bioelectronics applications that could benefit from using a hydrogel substrate, which is an intrinsically poor electrical conductivity. While the high water content favors an excellent ionic conductivity, electronic conductivity is required to interface with the external electronic equipment, in order not to compromise the performance of the device due to poor communication with the external equipment that is generally based on electron transfer[5] Up to now, the enhancement of the electrical properties of hydrogels still has strong limitations because, even if strategies such as including conductive components inside the gel matrix are being developed, the modification of the hydrogel composition

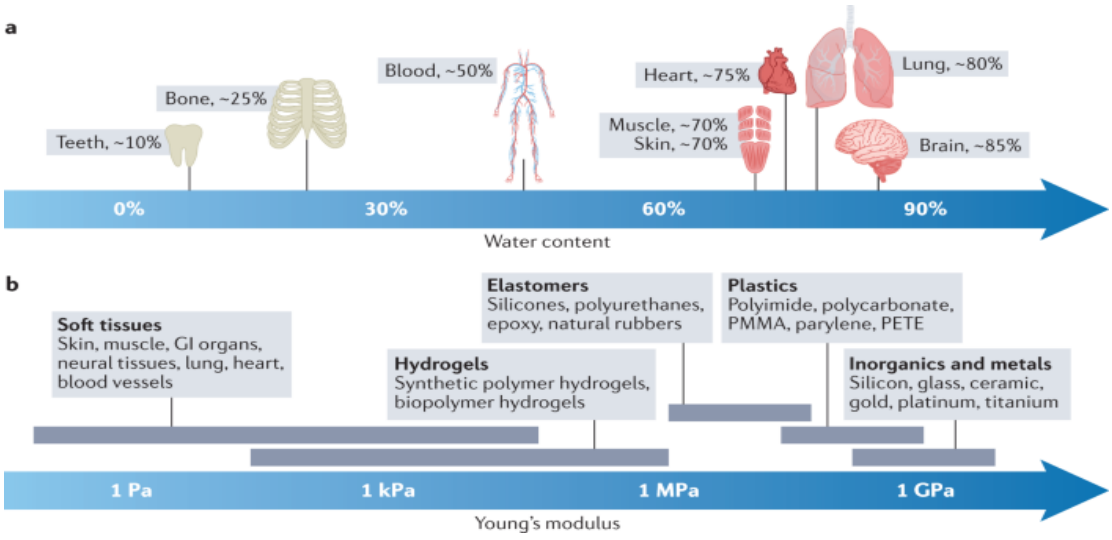

Figure 2.1: Biological tissues and hydrogels similarities, water content (part a) and Young's modulus (part b). Adapted from [2]. Copyright 2024, Springer Nature Limited.

often means compromising the mechanical properties of the material, and is still difficult to have a good spatial control over the conductive areas, so finding a strategy to achieve a significant and controllable electrical conductivity still remains a challenge.

2.2 Thesis objective

My thesis project will focus on the assessment of a new method to achieve and spatially control the electrical conductivity of hydrogels. The objective is to obtain conductive metallic structures embedded inside a hydrogel matrix. To do this we introduce silver ions inside the hydrogel and use the direct laser writing method to photo-reduce those ions and try to achieve electrical conductivity in the substrate. Moreover, the advantage of this method would be that the resolution given by the laser allows us to have high control of the spatial distribution of the metal structures and so obtain conductive features that are not just spread in the whole matrix, but that can follow a predefined, specific path and could allow to actually design a circuit in-gel, as shown in *Figure 2.2*. During my project I will study substrates characteristics, such as Young's modulus, strain at break and bonding properties with the silver ions, to establish the most suitable properties of the material for the process, then I will try to find a set of parameters for the direct laser writing method that are able to provide the best results in terms of conductivity and writing resolution, and finally perform an analysis on the electrical conductivity achievable with the written metal structures.
A possible final application would be to use the conductive hydrogels to sense or stimulate electrical signals related to neurons functioning in the brain, or to use them as substrate for cell culture that can allow to receive the response of the growing organoids directly from the substrate.

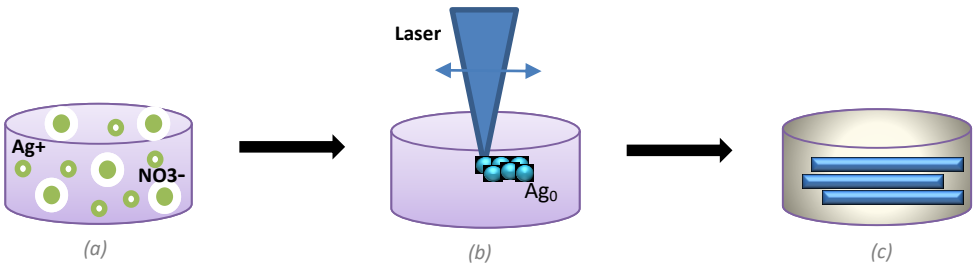

Figure 2.2: (a) Hydrogel matrix filled with silver ions, (b) photo reduction of the silver ions into metal particles using laser writing, (c) silver tracks written into the hydrogel.

3. Theoretical background

3.1 Hydrogel fabrication: state of the art

Hydrogels are materials composed of a network of hydrophilic cross-linked polymer chains that are swollen in aqueous solution. Polymer chains are a sequence of units called monomers that form long structures, which can be interconnected to each other to form a three-dimensional network. In the case of hydrogels, those chains are usually characterized by hydrophilic groups such as –OH, -COOH and $–SO_3H$ that give hydrogels the ability to uptake large amount of water. In the following, we will distinguish hydrogels between two macro-categories, one based on the source of the monomer, and the other one based on the crosslinking method.

3.1.1 Natural, synthetic and hybrid hydrogels

The polymer chains are the base of the hydrogel structure, and one of the main source is represented by natural polymers derived from plants and animals, like polysaccharides (cellulose, alginate and chitosan) and proteins (gelatin, collagen and elastin). One of the main advantages of using natural polymers is the non-toxicity, biocompatibility and biodegradability of the final hydrogel, which makes them ideal for biomedical applications. These properties come directly from the natural origin of the polymers that provide a high similarity to the extracellular matrix so that it is easier for cells to adapt to the hydrogel environment[5]. On the other hand, the drawbacks come from the low thermal stability and the mechanical properties, as naturally sourced hydrogels have lower strain at break than synthetic ones and it is difficult to increase their strength and flexibility. This limit can be overcome with synthetic polymers (Poly-ethylene glycol, Poly-vinyl alcohol, Poly-vinyl pyrrolidon, Poly-acrylic acid and Poly-acrylamide) that allow better control of chemical and physical properties, but of course, they have a limited biological affinity and are mostly non-biodegradable. Hybrid hydrogels try to combine the properties of the previous structures, using both natural and synthetic materials as a strategy to achieve mechanical strength and biocompatibility at the same time[6].

3.1.2 Physical and chemical crosslinking

The polymer chains, independently of their origin, have to be cross-linked to obtain a three-dimensional network. Hydrogels that form a crosslinked network upon ionic and electrostatic interaction, hydrogen bonding, hydrophobic and hydrophilic interactions, or metal coordination, are called physical hydrogels[6]. An example of physical gel are agar and gelatin, which undergo gelation when dissolved in hot water and then cooled down. The formation of the hydrogel network is made possible by weak interactions, such as hydrogen bonding and hydrophobic interaction, which make the crosslinking process reversible by tuning the operating conditions, such as temperature or pH. Interestingly, physical hydrogels exhibit self-healing properties, so when the gel is damaged the polymer chains can diffuse towards each other and when they come in contact at the broken interface, the dynamic bonds characterizing the network can re-form and restore the hydrogel matrix. The interaction between the polymer chains can happen thanks to opposite-charged molecules that are able to form a bond between each other and keep together adjacent polymer chains. Also temperature is a factor responsible for physical crosslinking, as a sol-gel transition can be triggered by a critical temperature, which allows the hydrophobic part of the micelle to aggregate together and form eventually the hydrogel. In particular, the LCST (lower critical solution temperature) polymers can form gels when the temperature of the solution is above LCST, while UCST (upper critical solution temperature) hydrogels are formed when the temperature goes below the critical one. Another common example of physical crosslinking is represented by the binding affinity between a metal ion and the functional groups present in the polymer that can connect the polymer chains together thanks to the addition of the metal in the hydrogel matrix[7].

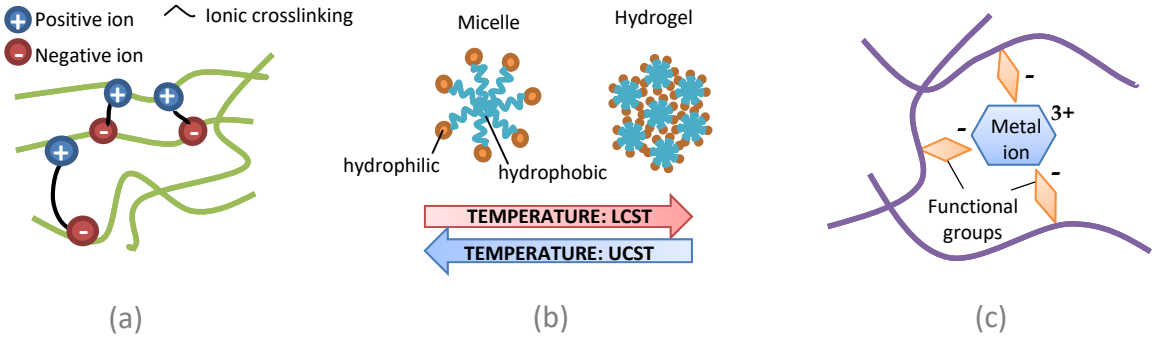

Figure 3.1: schematics of different physical crosslinking methods based on Ionic interactions (a), hydrophobic interactions (b) and metal coordination (c).

The mentioned crosslinking methods rely only on a physical interaction, hence they avoid the use of chemicals that can remain unreacted and lead to potential

toxic reactions, but they still can be harmful. For example, alginate is a biopolymer derived from algae that can form a gel form the precipitation that origins when is added to a calcium chloride solution. In this case the precipitate that is collected has to be rinsed several time to remove the chlorine ions that are still present in the gel and can cause unwanted reactions. The physical gel formation is however prone to create imperfections within the matrix, and the polymerization process is in general less reproducible and not easy to control as a chemical one.

A chemical crosslinking instead is based on non-reversible reactions that allow to have a better control over the mechanical and thermal properties. One common methods used to form the hydrogel matrix is by free radical polymerization, where an initiator is used to form free radicals inside the monomer solution thanks to the action of an external stimulus, which can be either light or temperature. Once formed, those radicals such as dangling bonds or unpaired electrons, are transferred to the monomer and to the crosslinker molecule, allowing to form covalent bonds within the polymer chains that can crosslink together to form the hydrogel network. Some common covalent hydrogels are for example PAM and PVA that are characterized by highly tunable mechanical properties and high reproducibility, also thanks to a controllable polymerization, and show irreversible crosslinking. The polymerization can be done also through "click chemistry", which uses reactions with high yield and selectivity involving functional groups to form the polymeric material. This can be achieved for example by Michael addition, where a nucleophilic molecule acts as a donor of electrons while an unsaturated carbonyl acts as an acceptor. When the solution is mixed under mild conditions, the addition reaction takes place forming a carbon-carbon bond between the polymer chains and it allows the formation of a covalently cross-linked network[5–6–7].

3.2 Mechanical properties

Mechanical strength is a highly investigated property in hydrogels to meet the requirements necessary for the variety of applications they are used for. In the biomedical field above all, the materials have to be able to biomechanically achieve the functions of the different tissues they has to interface with or replace, and to do so hydrogels have to cover a variable range of stiffness, as shown in *Figure 2.1*. The mechanical properties can be controlled by tuning the monomer and crosslinker concentration used to make the hydrogel. Fixing the monomer quantity, a larger amount of crosslinker will lead to a stiffer network, however, if the quantity is too high it will compromise the elasticity of the substrate and

become brittle. Hence to obtain a hydrogel suitable for applications that require both strength and flexibility, is essential to find an appropriate compromise between elasticity and mechanical strength[8]. These properties of the substrate can be quantified through the elastic modulus, and, as hydrogels are polymer networks swelled in an aqueous environment, those properties also depend on the swelling ratio of the material.

Materials deform when they are subjected to a load, and the stiffness represents the property of a structure to resist this deformation. The correlated property of the material is defined through Young's modulus (E) which is one of the most used quantities to characterize a material being independent of the structure. It is defined as: $E = \frac{\sigma}{\epsilon}$ (1). It is defined when the material is subjected to uniaxial stress, which can be both compressive and elastic, and measuring the corresponding deformation on the linear region of the stress-strain curve obtained[9], as evidenced in the blue zone in *Figure 3.2*. This deformation is called strain (ε) and is defined as the ratio between the change of length ΔL and the original length L_0, while the stress (σ) is the force per unit of surface, defined as the cross-sectional area which is perpendicular to the force.

Strain: $\sigma = \frac{F}{A}$ Stress: $\varepsilon = \frac{\Delta L}{L_0}$ (2)

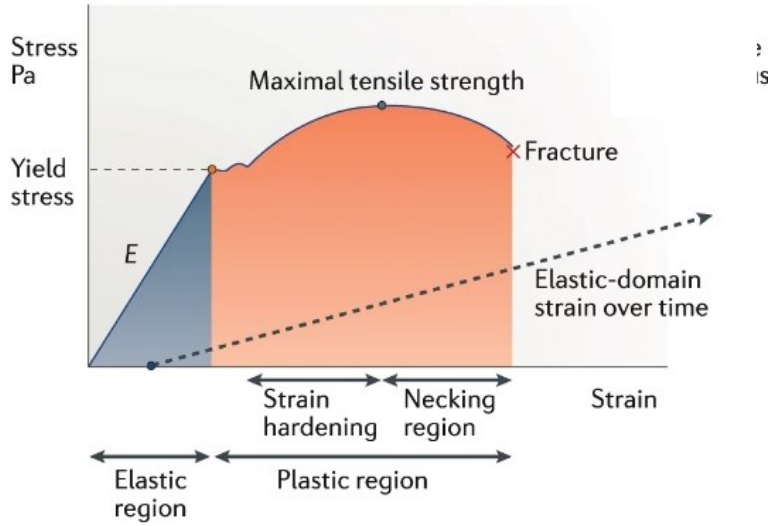

Figure 3.2: Stress vs Strain curve. Reproduced with permission[8]. Copyright 2024, Springer Nature Limited.

Moreover, hydrogels can uptake water and the change in volume and size of the substrate depends on the availability of hydrophilic groups, so the crosslinking degree affects also this property of the hydrogel that will tend to swell less if the network is highly crosslinked. The swelling can vary based on the liquid medium the hydrogel is surrounded by and can even result in a de-swelling if the material shrinks with respect to the initial condition. The main methods to quantify the swelling ratio are based on the volume and diameter change of the hydrogel with

respect to a starting condition, which is typically a dried sample, and is calculated as follows:

$$Q = \frac{Q_s - Q_i}{Q_i}, \tag{3}$$

Where Q_s is the weight (or diameter) of the swollen gel and Q_i is the initial weight (or diameter) of the gel before swelling.

All the mentioned properties can be used to characterize the hydrogel and quantify the effect of the changing of crosslinking and monomer content, crosslinking method, in order to meet the wanted characteristics for a specific application of the material.

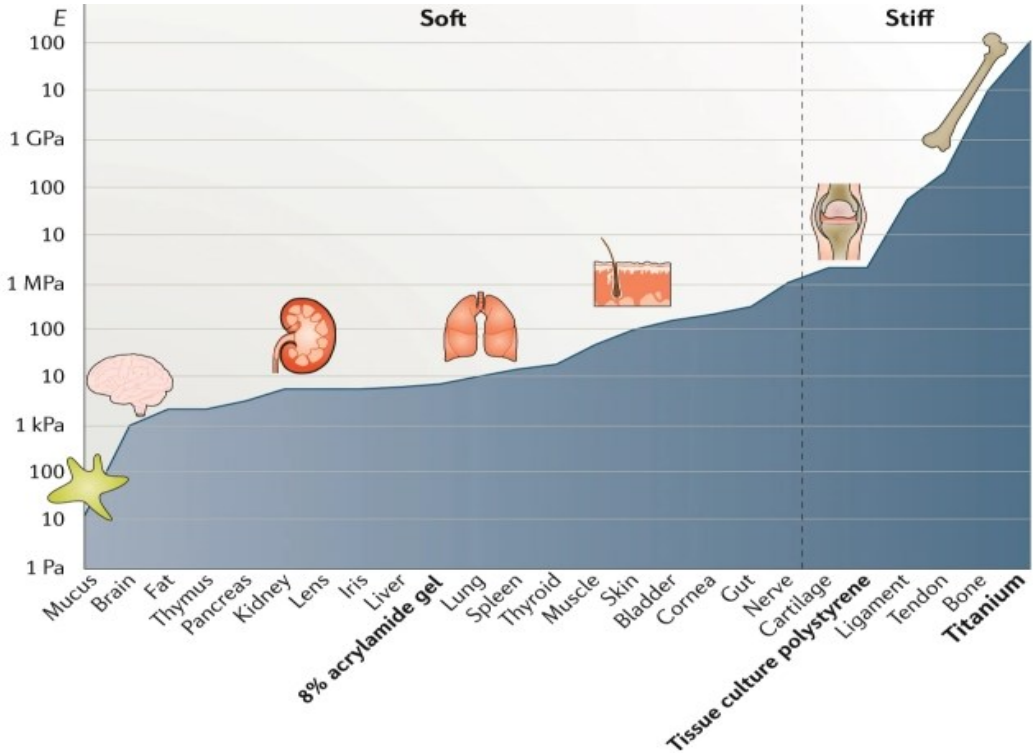

Figure 3.3: Young's modulus values of living tissues. Reproduced with permission[8]. Copyright 2024, Springer Nature.

3.3 How to make hydrogels conductive

The tissues composing our body show a moderate conductivity, around 0.001 to 100 S/m, which is mostly achieved through ionic fluxes[5-10-11]. Thanks to their water-based nature, hydrogels intrinsically present an ionic conductivity when swelled in an aqueous electrolyte. Methods to enhance ionic conductivity are based for example on the incorporation of ionic salts in the hydrogel matrix, or the use of polyelectrolytes to provide the conductivity thanks to their charged polymer chains. However, the main limitation with using ionic conductive hydrogels is that of interfacing the biological environment with the external electronic equipment[5]. Indeed, electrodes are the most spread strategy to record and send electrical signals to biological tissues, and they are based on electrical conductivity, which relies on electrons upon ions as primary charge carries. To obtain electrical conductivity with this kind of hydrogel, the salt content in the gel would be too high (>1 M) with respect to the ions concentration present in the physiological environment (<300 mM), leading to biocompatibility issues due to the diffusion of the salts in the cellular membrane, defined as osmotic imbalance. Hence the difference between the conduction mechanisms leads to a mismatch at the hydrogel/electrode interface that causes a high interfacial impedance and low charge injection capacity[5]. The different primary conducting species, i.e. ions and electrons, lead to poor communication with the equipment because the conversion form ionic to electronic signal inevitably causes noise and signal loss or distortion. To avoid this, it is necessary to achieve electrical conductivity in hydrogels, without compromising the compliance necessary for implantable electronics[12].

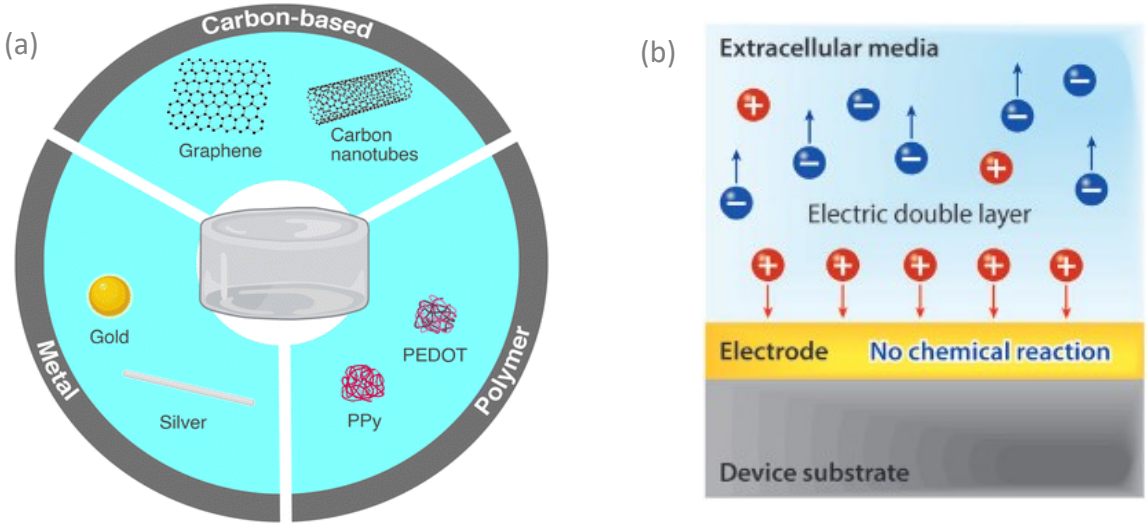

Figure 3.4: conductive nanomaterials to achieve electrical conductivity in hydrogels[4] (a). Illustration of the electrode/electrolyte interface[5] (b).

The most common methods used to introduce electrical conductivity in hydrogels are based on the introduction of conductive nanomaterials inside the gel matrix to achieve percolation. Percolation happens when inside the hydrogel the filler particles form a continuous network when they come in contact with each other, arranging in a particle cluster. Therefore, the percolation threshold has to be reached to ensure a significant conductivity of the gel matrix[4]. A widely used group of fillers are carbon-based nanomaterials, such as carbon nanotubes, graphene and carbon-black, thanks to their high electrical conductivity, mechanical strength and chemical stability in wet environments. The carbon-based materials are dispersed in the precursor solution before polymerization and a hydrogel with conductive carbon fillers is obtained. Typically, such conductive hydrogels show a conductivity in the 10^{-4}–10^{-2} S/m range, indeed to obtain higher conductivity values required by bioelectronics applications, the filler particles loading should be around 20 wt%. Such a high quantity of filler however becomes detrimental for the processing of the material, as it strongly reduces the strain at break, it increases the viscosity limiting the possibility to extrude the material, and additionally the fillers act as radical scavengers, so if the material is intended for UV polymerization the filler may interfere with the process by deactivating the free radicals necessary for the polymerization. Moreover, nano-sized materials can introduce inhomogeneity in the polymer chains, being larger in size, and fillers like carbon nanotubes have shown cytotoxicity due to their harmful interactions with the cellular membrane. To avoid this problem, some intrinsically conducting polymers have been explored. Conducting polymers are macromolecules characterized by alternating double and single bonds. They present delocalized π-bonded electrons that can be combined with dopant ions to enhance the charge-carrying ability. Some common conductive polymers are poly-(3,4-ethylenedioxythiophene) (PEDOT), polypyrrole (PPy) and polyaniline (PANI), they are generally biocompatible and not difficult to process, but their brittleness can reduce the mechanical properties of the hydrogel matrix[4]. Metal nanoparticles are another type of electrically conductive fillers that are embedded into the hydrogel matrix as pure metal oxides and lead to high electrical conductivity, as described in the previous methods. Even if they show good conductive and also antibacterial properties, the disadvantage is that they are more expensive compared to the previously mentioned materials and not completely chemically inert, for example they can be oxidized when placed in an aqueous environment.

Despite of good electrical conductivity enhancement obtained through the described methods, adding fillers in the precursor solution still alters the rheological properties of the hydrogel, such as viscosity, elastic modulus and yield stress. Moreover, the distribution of the nano-materials inside the matrix is

not controllable, as the fillers are dispersed in the whole hydrogel without following any spatial localization. The conductivity obtained with those methods is a great result for the bioelectronics field, but it still strongly depends on the percolation threshold, which is reached only with high concentrations of fillers at the expense of the hydrogel properties. Therefore, a forward step in the research would be to obtain high conductivity through a localized percolation path inside the hydrogel that limits the amount of fillers, so that the alteration of the rheology of the matrix can be contained without giving up on the electrical properties.

3.4 Two-photon direct laser writing

The interest in fabricating nano-sized metallic structures has increased in the last years, and researchers wanted to find a method to achieve high throughput and resolution, alternatively to the lithographic processes mostly used for nanofabrication. Direct laser writing has therefore gained a relevant position thanks to its fast and controllable writing properties that allow to create 3-dimensional structures in a one-step process. The direct laser writing process involves the photoreduction of a metal precursor into metal nanoparticles, triggered by two-photon absorption. This process occurs when a light source, in this case, the laser beam, provides energy to the system and excites a molecule to a higher energy state. Unlike the one-photon absorption, which involves the absorption of a single photon and can occur throughout the entire volume exposed to the light, two-photon absorption requires the simultaneous interaction of two photons, each of lower energy, making it a non-linear process. This means that the process occurs with a probability that is proportional to the square of the light intensity, so the excitation region is limited to a small focal volume where the photon density is sufficiently high. This intrinsic localization is essential for 3D lithography, as it allows for precise control over the spatial position where the photoreduction occurs, enabling the creation of complex three-dimensional structures. For the process to take place, the wavelength of the laser is chosen so that the amount of energy delivered to the molecule is equal to the difference between the two energy states of the molecule to make the transition of the photons to the excited state happen[13]. The laser is focused into a solution containing both metal ions and a photoinitiator. This molecule is able to absorb the two-photons and when it transitions to the excited state can generate free radicals, which are highly reactive species. The radicals will then interact

with the metal ions by donating electrons so that the metal cation reduces to a zero-valent molecule. Once the ion is reduced it exists as a single atom, and the number of the reduced atoms found in the focal volume of the laser needs to reach a certain threshold number to allow the nucleation process to happen. When the atoms join together to form a stable nucleus, the growth mechanism can start, as further reduced atoms will now form around the already existing particles. The growth is driven by the Ostwald ripening, which is a spontaneous process favoring the formation of larger particles upon smaller ones. Indeed, particles that are bonded to fewer atoms are less stable than ones having a higher number of bonds, hence the system will try to have a lower overall energy and this causes smaller particles to redissolve and favor the growth of larger ones, which shows a lower surface energy[14,15]. The reduction process followed by the nucleation and growth leads finally to the formation of metal nanoparticles.

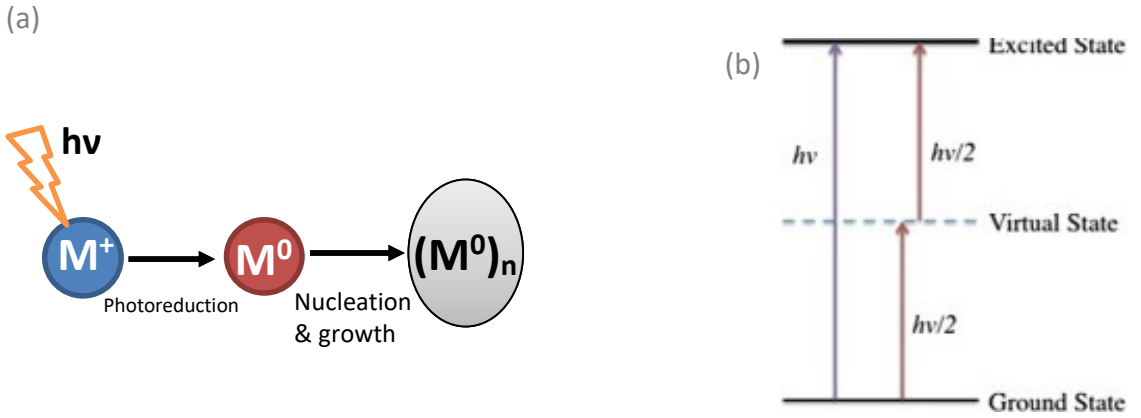

Figure 3.5: Schematic of the nanoparticles formation process from the ion precursor (a). Schematic of the two photon absorption process from ground state S_0 to the excited state S_1 (b). Adapted from[14]

The existing studies using two-photon reduction as a writing technique for three-dimensional metallic structures can be distinguished into two categories based on the fabrication materials: the first one using metal-ion aqueous solutions, and the second one using doped polymeric resins. In the first case metal salts are dissolved in an aqueous solution that is directly placed on a cover slip. Then the laser beam is focused inside the solution and is able to reduce the metal ions to form self-standing structures. In the second method a polymeric resin is used in addiction, so the laser triggers at the same time the photoreduction of the ions and the polymerization of the resin. Indeed the polymeric matrix that forms around the designed structure allows to achieve more stability, as the rigidity of the polymer prevents the ion diffusion and the collapsing of the feature. Tanaka et al.[16] were able to achieve self-standing 3D conductive structures using an aqueous solution of silver nitrate, with the addition of a photoactive component. The solution is placed between two cover slips and the laser beam is focused into it to create the metallic structure upon photoreduction. The final design with a

0.7 µm resolution and a conductivity of the order of 10^{-8} Ω·m is obtained on the glass cover. Other groups like Maruo et al.[17] and Waller and Freymann[18] used polymeric films as precursor materials. In this case, the photopolymerization of the matrix and the formation of the metallic structure happen at the same time. The silver feature is encapsulated into the polymer that is then washed away to achieve the final structure.

Until now, the conductive structures obtained are therefore achieved as free-standing features, and polymeric matrix is used only as a sacrificial layer to help support the design during the writing. Yet, no conductive elements embedded into a gel matrix have been reported yet in the literature using the direct laser writing method. The novelty of the project studied during the thesis is that the metallic structures are written in a pre-crosslinked hydrogel matrix, which is not washed away after the process. The silver features remain encapsulated in the gel, introducing electrical conductivity. Thanks to the precise focus of the laser beam, the conductivity is not spread into the whole matrix but is achieved in a spatially-controlled way.

Substrate	Supporting matrix	Resistivity	Reference
Glass	No	10^{-8} Ωm	16
Glass	Yes, Photoresist	10^{-8} Ωm	26
Glass	Yes, PVK	10^{-5} Ωm	24
Gelatin	Gelatin, removed after DLW	10^{-4} Ωm	25

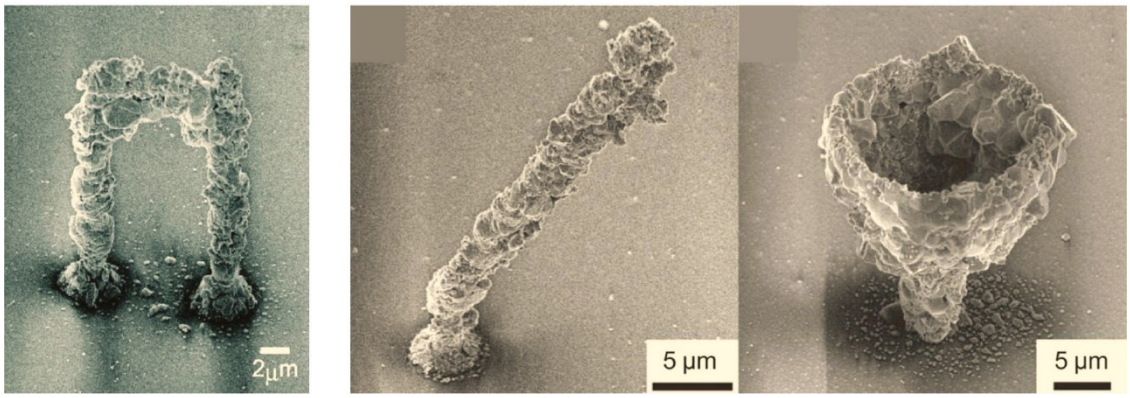

Figure 3.6: table of resistivity for silver structures made with direct laser writing found in literature. Pictures of free-standing silver structures obtain through direct laser writing technique[16].

4. Materials and methods

Materials used for the experiments:

[2-(Methacryloyloxy)ethyl]dimethyl-(3-sulfopropyl) ammonium hydroxide (DMAPS) (Sigma, 537284), Acrylic acid (AA) (Sigma), 2-Acrylamido-2-methyl-1-propanesulfonic acid (AMPS) (Sigma, 102131190), Acrylamide (AM) (Alfa Aesar), Metylene bisacrylamide (MBAA) (Carl Roth, 7867.1), 2-Hydroxy-2-methylpropiophenone (PI) (Sigma, 405655), Phosphate-buffered saline (PBS) (Sigma, P5368), Glycerol (Thermofischer, 7530.1), Silver Nitrate ($AgNO_3$) (Carl Roth, 9370.4), Deionized water (Drect-Q) with a resistivity of 18.2 MΩ/cm.

4.1 Preparation of hydrogel substrates

The substrates used for the direct laser writing process are based on four different monomers, characterized by distinguished functional groups. Acrylic acid (AA) is a negatively charged monomer that contains the carboxylic group $-COOH^-$, acrylamide (AM) which contains the amide group, (2-Acrylamido-2-methyl-1-propanesulfonic acid) (AMPS) that is negatively charged, and [2-(Methacryloyloxy)ethyl]dimethyl-(3-sulfopropyl) ammonium hydroxide (DMAPS) and that present a sulphonate group and is zwitterionic. The mentioned functional groups have the ability to bind to metal ions, which ideally helps the localization of the nanoparticles formed through the photoreduction process. The selected monomers are also biocompatible and can be polymerized easily through a UV crosslinking method. Moreover, zwitterionic monomers have antifouling properties, given by their highly hydrophilic nature and thanks to the fact that they have an overall neutral charge because the number of anionic and cationic groups along the chain is the same. The combination of these two properties prevents indeed the proliferation of bacteria and the binding with proteins, making them good candidates for biomedical applications.

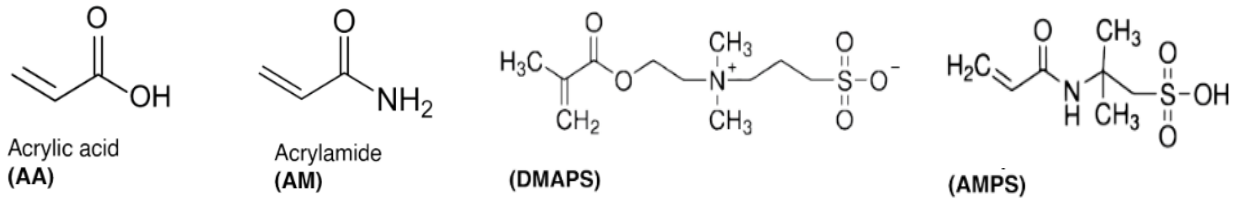

Figure 4.1: monomer molecules.

4.1.1 DMAPS substrate preparation procedure

To prepare the hydrogel substrate we use an aqueous solution containing 60 wt% DMAPS monomer, 0.6 mol% of MBAA (Methylenebisacrylamide) crosslinker and 5 µL/mL of PI (2-Hydroxy-2-methylpropiophenone). The monomer mass ($m_{monomer}$) expressed in milligrams is calculated from the molecular weights of the molecules($M_{w\ MBAA}$ and $M_{w\ monomer}$), given in g/mol, using the following expression:

$$m_{MBAA=} \frac{m_{monomer} \times M_{w\ MBAA} \times mol\% \times 1000}{M_{w\ monomer}} \quad (4)$$

The DMAPS monomer is mixed with water, then the MBAA is added and mixed until the crosslinker is fully dissolved. Being MBAA poorly soluble in water it might be necessary to sonicate the solution in the ultrasound bath to help the dissolution. The solution is then wrapped into an aluminum foil to avoid contact with light, and the PI is added. Before the polymerization, we perform degassing for 5 minutes to replace the oxygen present in the solution with an inert gas, in our case nitrogen, to avoid that during the polymerization the oxygen acts as radical scavenger, compromising a regular and reproducible polymerization of the gel. The solution is then poured between a 500 µm thick rectangular mold and a glass slide, to avoid evaporation and achieve a smoother surface. The solution is cured in a UV oven for 5 minutes with an intensity of 25 mW/cm^2. After the polymerization, the hydrogel substrate is detached from the glass and left to rinse in water for 24 hours, to remove any residual unreacted species from the matrix before use.

Monomer	Monomer wt%	Crosslinker mol%
DMAPS	60	0.6
AM	40 20	0.4
AA	40	0.6
AMPS	30	1.2

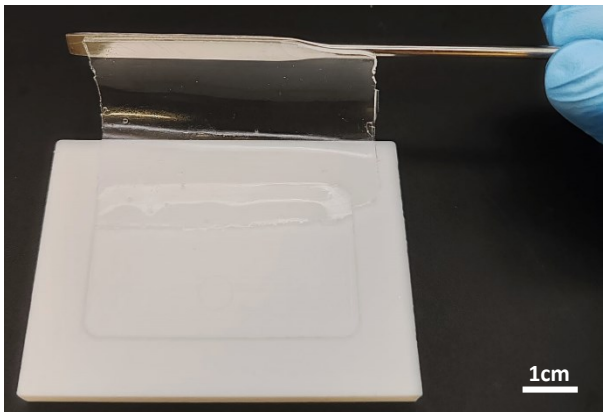

Figure 4.2: In the table a summary of the monomer and crosslinker concentrations is shown. In the picture a PDMAPS substrate removed from the mold after UV crosslinking.

Substrates based on different monomers are prepared following the same protocol, adapting the crosslinker mass to the respective monomer molar mass value. The acrylamide was prepared with 40 wt% and 20% monomer and 0.4

mol% MBAA, the acrylic acid monomer weight was 40 wt% with 0.6 mol% MBAA, while AMPS concentration was 30 wt% and MBAA 1.2 mol%.

4.2 Mechanical characterization of the substrates

4.2.1 Universal testing machine

The mechanical tests on the substrates are performed with a Universal Testing Machine (UTM), which is able to perform tensile, compression, flexure and other mechanical tests on a large variety of materials. It is composed of a crosshead for the up and down movements, and a load cell, which allows to measure the force required to deform or break the material. An extensometer is used to measure the strain that occurs in the sample when subjected to the pulling force. The samples are connected to the machine through a pair of grips that transfer the movement of the crosshead to the specimen. For our tests the screw grips have been selected as they allow a manual and gentle control over the holding strength that has to be sufficient to avoid the sample to slip off the grips, but not too high or the hydrogel would break[19]. The system is controlled through a software that allows to set the desired parameters such as the maximum load force, which is in our case 50 N, the speed at which the force is applied that is 100 mm/min and the geometrical measurements of the sample that allow to obtain the direct calculation of the Young's modulus value.

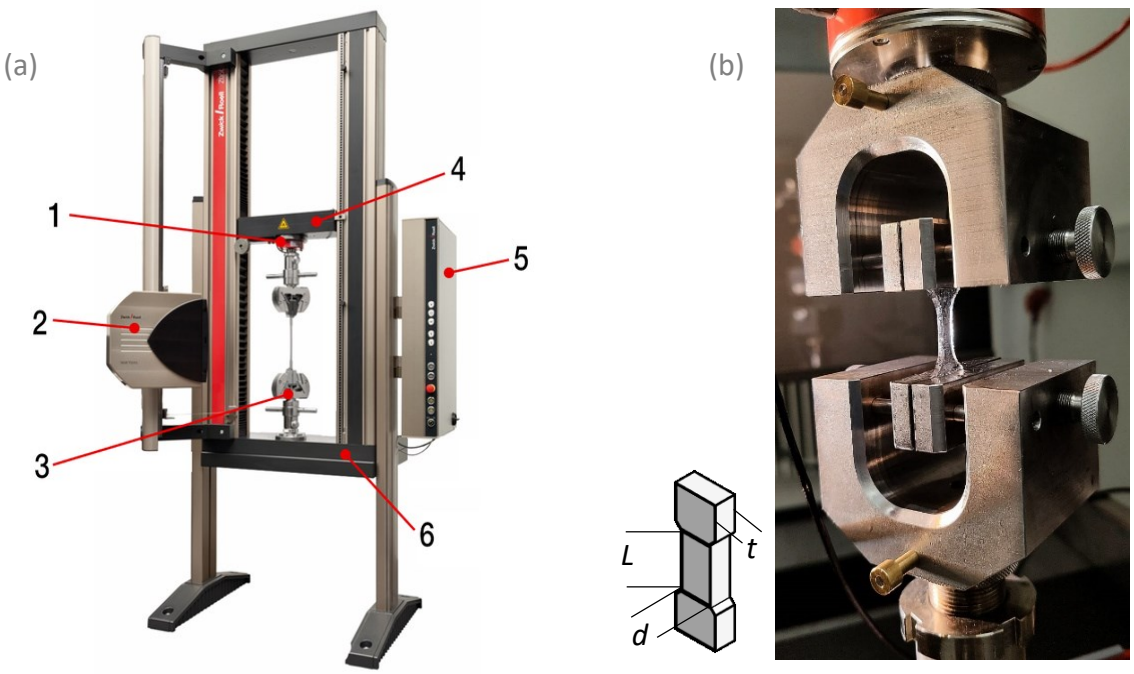

Figure 4.3: (a) UTM used for the tensile tests: 1. Load cells, 2. extensometer, 3. specimen grips, 4. crosshead, 5. electronic control, 6. driving system[17]. (b) DMAPS sample during the tensile test.

The samples on which we perform the tensile test are prepared with the same protocol described in section *3.1*, and are casted in a dog-bone shaped mold that present two larger extremities which are inserted between the grippers, and a central rectangular part which is stretched by the applied force and deforms uniformly until break. The test is performed on an average of 4 samples for each substrate and condition, and are soaked at equilibrium both in water and in a 1:1 PBS/Glycerol solution that is the same environment in which the electrical measurements on the gels are performed. The samples to test are taken out from the liquid and are placed right after between the grippers, so the hydrogel does not dry out and change its mechanical properties. The test is then started and the sample is pulled by the force until the breaking, which have to occur in the middle of the sample to provide a valid result. The strain percentage with the corresponding value of the applied force is measured by the machine, so we can perform a straightforward calculation of the stress and strain parameters by using the force and the geometry of the sample as described in section *2.2*.

4.2.2 Swelling ratio

The swelling ratio measurements of the substrates are performed on circular samples of 0.6 mm radius. The samples are dried in the oven at 70°C for one hour and the initial weight is measured with a precision balance, while the radius is evaluated with an electronic caliber. Then the samples are placed in a well plate and left to swell in 1 mL of the liquid medium for which we want to calculate the swelling parameter, which are water, the 1:1 PBS/glycerol solution and the aqueous silver nitrate solution. New measurements of both weight and radius, are taken after 1 hour, 2 hours, 24 hours and 48 hours after the first measurement in the dry condition. The excess of liquid is removed with the aid of a Kim wipe before weighting to avoid discrepancies due to the influence of the volume of liquid present on the surface and not just inside the gel matrix. For each different swelling medium, three samples are measured for each substrate.

4.3 Nanoscribe Photonic Professional GT+

4.3.1 Equipment description

The Nanoscribe Photonic Professional GT+ is a 3D nanoprinter that uses two-photon absorption triggered by an infrared femtosecond laser operating in the infrared range (λ=780 nm) to polymerize UV-sensitive materials, most commonly photoresists. A microscope objective allows to direct the light

intensity of the laser at the focal point and reach the threshold sufficient to trigger the two-photon absorption mechanism. The available objectives have different magnification and operating modes: a 20x objective working in air, a 10x objective with a numerical aperture of 0.3 for macroscale mode, a 63x objective with a 1.4 numerical aperture for high-resolution mode and a 25x objective with a numerical aperture of 0.8, the last two both working in oil immersion to allow an optimal matching with the refractive index of the substrate.
The working distance of the 25x objective in oil immersion mode is 360 µm, yielding a maximum height for a structure that can be written inside the substrate is around 190 µm.

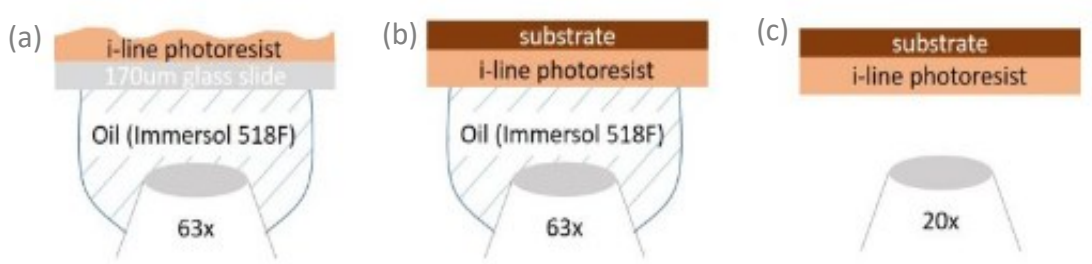

Figure 4.4: microscope objectives working in different modes (a) oil immersion through glass, (b) oil immersion, (c) in air[18].

The choice of the objective influences the scanning speed and the dimensions of the voxel, which can be defined as a 3D pixel that is scanned through the substrate. For our application, we use the 25x objective that provides a voxel with an oval shape of a maximum size around 600 nm on the x/y-axis and 2 µm on the z-axis. The voxel is scanned through the substrate, which is placed on a sample holder, using three principal displacement methods. A coarse stage allows to switch between different exposures fields with a precision of about 1.5 µm, while a piezo stage is used for high-precision movements during the writing process along the x, y and z axis with a 300 µm travel range. The last option is represented by the "GalvoScan" mode, which takes advantage of the positioning

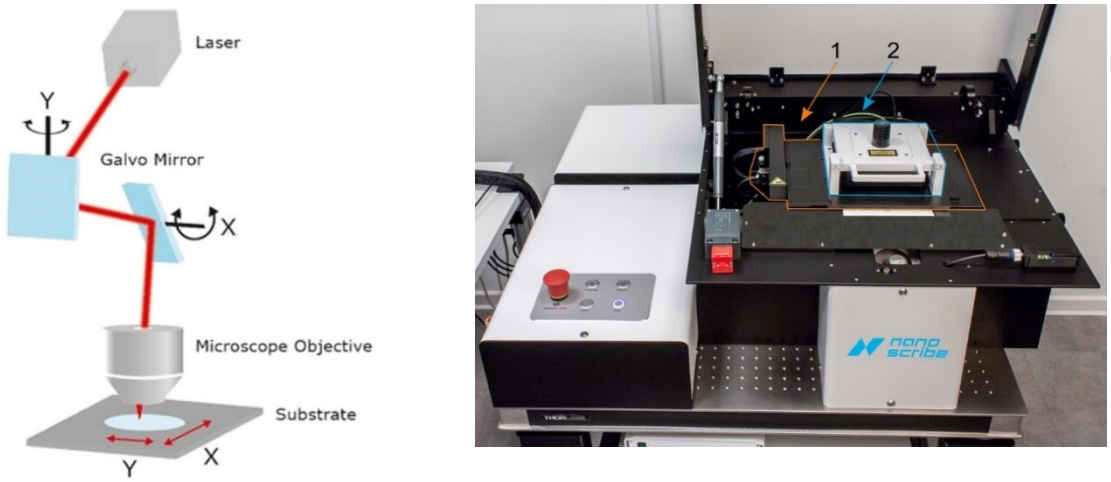

Figure 4.1: laser path for the Galvo mode (a), printing chamber with piezo-stage (b) [19].

of galvo mirrors to change the focal point along x and y directions, allowing a faster displacement compared to the piezo-stage if a very high resolution is not fundamental for the writing[20].

4.3.2 Writing parameters

The Nanoscribe is interfaced with a software that takes as input the design of the structure which have to be designed by the laser, and it allows to set the main control parameters, such as laser power, scan speed, slicing distance and hatching distance. The combination of these parameters influences the writing resolution and the efficiency of the photoreduction process.

Laser power (LP) indicates the laser beam's energy, allowing it to control the energy delivered to the substrate during a pulse. It is selected as a percentage of the maximum power when in continuous mode operation and can range from 0 mW to 50 mW when 100% laser power is selected.

Laser scan speed (SS) is defined in µm/s and defines the speed at which the laser is scanning a selected area. It has a great influence on the thermal effects developed into the substrate, as at lower scan speed the area exposed during each pulse is smaller and this leads to an increase of temperature at the irradiation spot[21]. Hence the combination of laser power and scan speed is a crucial element for having sufficient energy to trigger the photon absorption, but at the same time to avoid an excessive temperature that can cause oxidation or evaporation of the species present in the substrate. To avoid undesired effects due to overheating, a change in the laser power can be compensated by a change in speed, and the relationship between the two can be expressed through a quantity called laser dose:

$$D = \frac{(Pp)^2}{v}, \tag{5}$$

where Pp is the incident power of the pulsed laser used to trigger the photoreduction mechanism, and v is the laser scan speed. The dose however is just an indicative parameter, as during the writing process there are multiple factors dependent on the substrate and the interaction with the metal ions that influence the quality of the printed structure. One phenomenon that can cause a destructive effect on the writing is the formation of microbubbles due to the structure-light interaction that leads to the boiling of the solvent[22].

Slicing distance and hatching distance are the last two important design parameters. As introduced in the previous section, the Nanoscribe uses a set of galvo-mirrors and a piezo-stage to move the laser through the structure. To optimize the writing process, the design is divided into slices along the z-axis so

that the writing is performed layer by layer and the slower piezo-stage is moved only once all the features on the same z-plane are complete. The distance between each of these layers is called **slicing distance**. Ideally, if the slicing distance is greater than the voxel size on z, which is 2 µm, there is no contact between two consecutive layers, while if this distance is lower than the voxel size there is an overlap of the slices placed on a different z-plane. At the same time, the laser moves on the x and y-axis and scans a single layer following a path of consecutive straight lines. The distance between two lines is represented by the **hatching distance**. The value of these two parameters also influences the writing. For example, if high slicing and hatching distances are selected, the nanoparticles will form less close to each other during the scans leading to a lower density of the structure. In terms of heating effects instead, a very small distance between the lines can favor the increase of the local temperature because the laser focuses on two areas that are very close in a short amount of time, so the dissipation of the heat is more difficult to achieve than in a less dense structure. The combination of laser power, scan speed, slicing distance and hatching distance allows us to define the general parameters for the writing process of the Nanoscribe, and their selection defines the quality and the timing of the process.

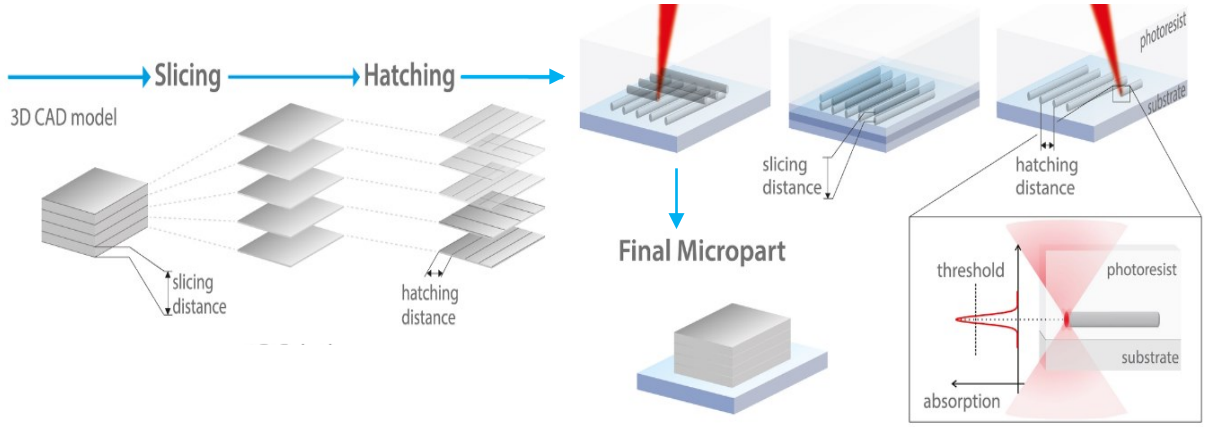

Figure 4.6: Schematic of the writing process with slicing and hatching distance representation. Adapted from[21].

4.3.3 Preparation of hydrogel substrate for direct laser writing

To prepare the hydrogel substrates for DLW, bulk hydrogels are punched in 8 mm diameter disks and dried in an oven at 70°C for 30 minutes. The precursor solution is prepared with 1:1 (by volume) water/glycerol solution as solventand 1M concentration of $AgNO_3$ as metal salt. Afterwards 10 µL/ml of photoinitiator (PI) are added to trigger the photopolymerization. The dried substrates are left to swell in the precursor solution in a well plate covered with an aluminum foil and stored in the fridge at 4°C. The samples must be at swelling

equilibrium in the metal precursor solution before the writing process, hence the substrates have to be prepared and left to soak in the $AgNO_3$ aqueous solution for 48 hours before using them for the direct laser writing process. After the writing, the samples are rinsed in water for 48 hours to remove the remaining silver ions inside the gel matrix and afterward, they are stored in a 1:1 glycerol/PBS (Phosphate-buffered saline) solution that is the final condition on which the electrical measurements are performed.

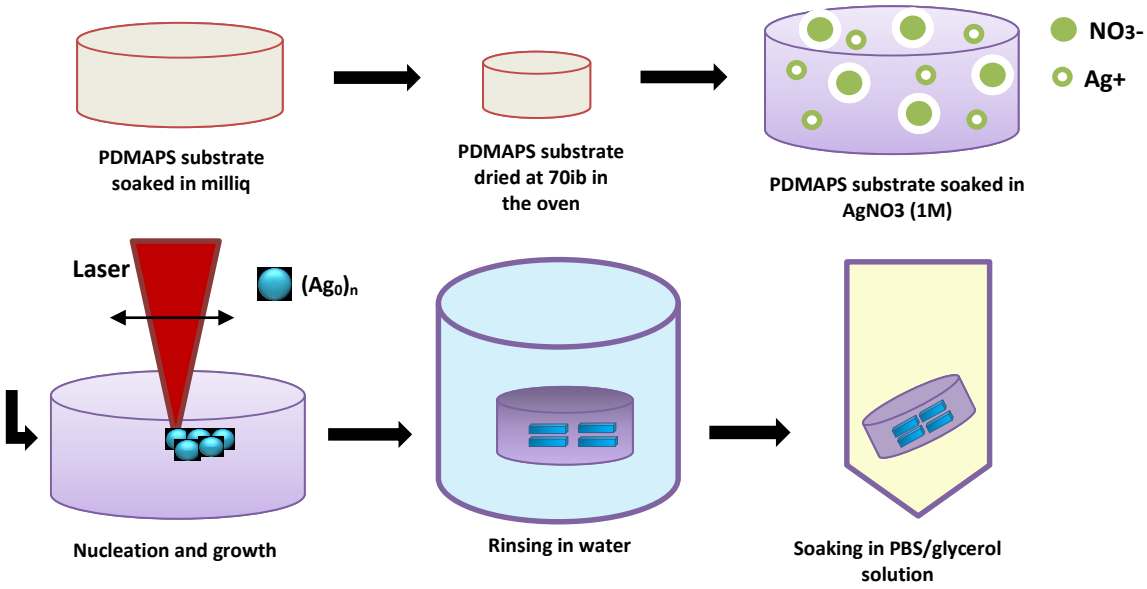

Figure 4.7: schematic of the silver structure writing process flow.

4.4 Electrical measurements

The electrical measurements are performed using a probe station on metal tracks embedded into the hydrogel matrix. The hydrogel previously soaked in the glycerol and PBS solution, is taken out from the liquid environment and placed on the holder of the probe station. A camera is placed above the sample and allows to focus on the features present inside the gel. A two-probe measurement is performed on a single track, so the probe tips of 50 µm tip diameter are put in contact with the two extremities of a rectangular track. Initially, a constant voltage is applied continuously with a Keithley 6517A voltage supply and the current is monitored to help find the right contact point. The probes are moved inside the gel in the x, y and z directions with the help of micromanipulators, and when they are correctly placed on the track, a peak of current is measured by the electrometer that indicates the presence of electrical conductivity. Then, to perform the electrical measurement, a voltage difference is applied between the extremities, performing a total sweep between -100 mV

and +100 mV. The applied voltage is of the order of millivolts to keep it below the water electrolysis potential, which is around 1.23 V. Indeed, the features inside the hydrogel are surrounded by an aqueous environment, so when the voltage is applied, a current is flowing both in the metal and in the electrolyte, and if the electrolysis potential is reached, this phenomenon can cause the unwanted generation of H^+ and OH^- ions by water splitting, which can lead to metal corrosion or possibly trigger other reactions. The applied voltage difference leads to the generation of an electric field, and the charges inside the sample are moved towards the direction of the electric force that is applied to them. The current that flows between the extremities of the track is measured by the electrometer (Keithley 6517a) and following Ohm's law, the resistance is obtained through the slope of the voltage versus current curve. Two properties of interest to be measured on the silver structures are the resistivity and the conductivity, which represent respectively the resistance to the flow of the current inside a material, and the ability to allow the flow of electrical charge[4]. The resistivity and conductivity of the tracks can be calculated with the following equations:

$$\rho = \frac{R \times A}{L} \qquad \sigma = \frac{1}{\rho}, \tag{6}$$

where R is the resistance, A is the cross-sectional area and L is the length of the track. When measuring the resistance, we have to take into account the fact that the two-probe method does not decouple the contribution coming from the contact resistance from the interface between the cables and the tips. If the electrical results showed a resistance comparable to the contact resistance, this value would have to be separated from the measured value by using a 4-probe setup.

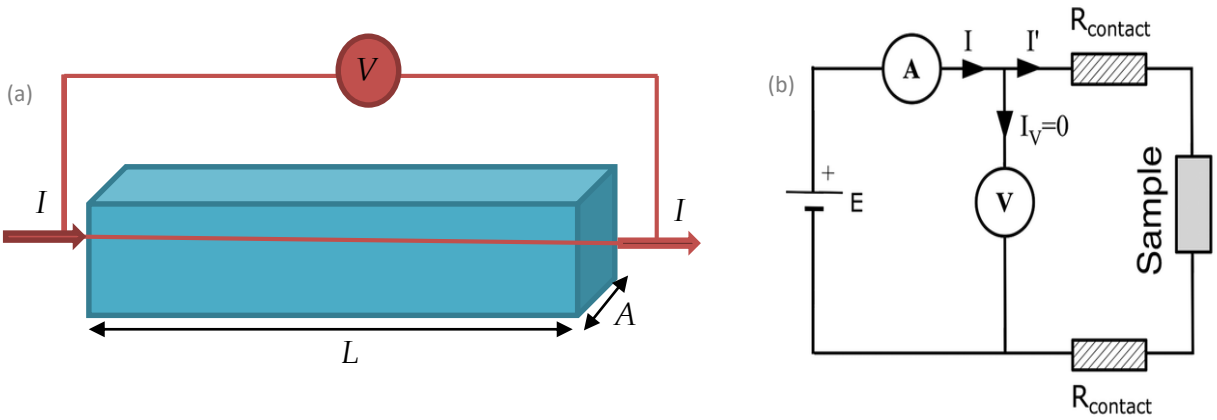

Figure 4.8: schematics of the two probe method on a rectangular track (a). Circuit diagram of two-point probe measurement (b). Adapted from[4].

The reference values for bulk silver are $1.59 \cdot 10^{-8}$ Ωm for the resistivity and $6.30 \cdot 10^{7}$ S/m for the conductivity[23]. In literature, several values for the resistivity of structures achieved with direct laser writing and 3D printing have been reported. The methods used to write the features in those cases are the ones described in *section 2.4*, so even if the two-photon absorption process is similar to the one we use in our project, the final structures are not embedded inside the hydrogel, hence most of the electrical measurements are performed with direct contact of the features with the tips or the electrodes, without the interference of the gel matrix that surrounds the metal. The resistivity measured in a work for structures made in polyvinylcarbazole (PVK)[24] has reached a value with the order of magnitude around 10^{-5} Ωm for measurements performed both with and without the sacrificial polymer, Komori[25] could measure a resistivity of 10^{-4} Ωm for features written in gelatin, Waller[26] et al. could measure a resistivity of 10^{-6} Ωm on their 3D silver microstructures written inside gelatin and a resistivity of 10^{-8} Ωm for structures measured on glass, while the group of Tanaka[16] could obtain a resistivity in the order of the bulk silver for free-standing features without a surrounding polymer. The cited works in most cases achieved at least two orders of magnitude higher resistivity than the one of the bulk silver because the surface presents overall some roughness, small voids can be created inside the structure causing some discontinuities and oxidation can occur at the surface, due to the aqueous environment around the silver particles during the writing. The presence of these factors even in small amounts can cause a significant increase in the resistivity of microsized features, so it is still difficult to obtain a good conductivity value that can reach the one of bulk silver and only very few groups could manage to fulfill this goal. Indeed most of the groups in the literature that use direct laser writing to realize 3D structure were not able to extract a significant conductivity value due to those artifacts that prevent having a continuous design.

4.5 Analysis of written structures

The silver structures that we write inside the hydrogel have dimensions ranging from tens of micrometers to couples of millimeters, and being able to quantify their dimensions after the writing process is fundamental to perform a writing resolution analysis and calculate the values of the resistivity and conductivity, as described in the previous section. To analyze the length and width of the features we used an optical microscope to take pictures of the sample after the writing, after the rinsing in water and after soaking in the PBS/glycerol solution. With the aid of the ImageJ software we then quantified the dimensions of the features for every step.

4.5.1 Micro-computed tomography

To perform an analysis on the thickness we used the Micro-computed tomography as imaging tool. Moreover a Micro-CT scan allows to have an insight on the density of the structure that is a useful information for us to see from the reconstructed image if the structure that we obtain is continuous or not. Indeed if percolation is present along the feature, we can see a uniform metal layer inside the gel that interconnects the structure from the top to the bottom following a conductive path. In case percolation is not likely to happen, we would see some voids that interrupt the silver path along the track and prevent it to be electrically conductive. Micro-computed tomography, or Micro-CT, is an imaging tool that allows the reconstruction of a 3D image combining the two-dimensional slices of a sample taken consecutively with the use of X-rays. This technique is non-destructive and makes it possible to have a high-resolution visualization of both the external and internal parts of the scanned feature. The reconstructed image can be manipulated on screen and simple volume and length measurements can be done, as well as density, porosity analysis and other material-related characterizations, without damaging the sample. The instrument's main components are an X-ray source, a sample manipulator and an X-ray detector. The sample is placed on the manipulator that is placed as close as possible to the source to get a greater resolution, and it performs a 360° rotation around the y-axis during the scan process. The X-rays are sourced inside a vacuum tube where an electron beam is generated from a filament and accelerated by a voltage difference. The beam is then focused onto a tungsten target and this interaction leads to the formation of X-rays. The nucleus of the target is able to decelerate the electrons and an X-ray photon is emitted as a consequence of the conversion of the kinetic energy of the electrons. This 'braking radiation' phenomenon gives

origin to the continuous X-ray energies spectrum that has a range between 0 and the voltage reached by the source, which can go up to 240 kV[27]. The X-rays are directed through the sample and an attenuated radiation arrives at the detector that converts the absorbed beam into light thanks to a scintillator screen. The light is converted by a CMOS or CDD camera into a projection image that is a 2D radiograph of the sample composed of thousands of pixels, whose values derive directly from the X-ray radiation measured through the detector. The acquisition is based on a 16-bit grayscale, where the darkest parts are referred to as the maximum absorption and the lightest ones correspond to a lower absorption, which is the minimum when the X-ray is passing through air. At the end of the process hundreds of 2D projection images are recorded and with a 3D reconstruction is possible to get a final volumetric representation of the sample[28]. The sample for the Micro-CT scan are prepared by cutting a single silver structure from the sample. The piece of gel is place vertically inside a pipette tip, immersed in the PBS/glycerol solution and is placed on the sample holder. The X-ray Micro-CT is performed with an Ultratom micro tomography system (RX-SOLUTIONS). The samples are scanned with a voxel size of 0.0009 mm, an applied voltage of 80 kV and a current of 140 mA.

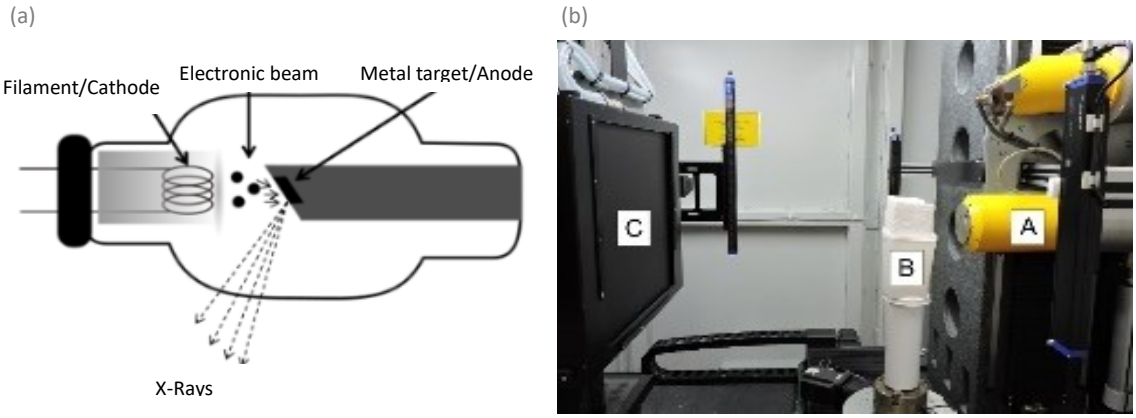

Figure 4.9: X-ray generator schematic(a)[24]. Micro-CT picture with the source A, sample holder B and detector C (b)[23].

4.6 Ring resonators

4.6.1 Working principle

A ring resonator is a closed-loop path resonator that allows electromagnetic waves to travel within the structure following a specific pattern. We want to design and test such resonators to detect the power absorption around the resonance frequency of the device embedded inside the hydrogel.

We use a vector network analyzer (VNA) to excite two-port systems in radiofrequency working in transmission mode. Power is sent as input to port 1, it passes through the device under test (DUT) and is finally read back as output at port 2. Knowing the input power we can calculate the amount of power that is transmitted to port 2 when we excite the system at different frequencies. The maximum output value corresponds to the 100% of the power given at the input when all the power is being transmitted, while around the resonance frequency, the output power starts to decrease and it can reach a minimum value of 0% in the ideal case where the electromagnetic field created around a specific frequency goes in resonance with the resonator, which is able to absorb all the provided power. When we work in radiofrequency the system behaves like a wave, hence the DUT works at frequencies high enough so that the electronic signal can undergo reflection or transmission when an interface is found. Every mismatch present along the line can interfere with a proper reading of the parameters, so to minimize the reflection of the power we have to try to have the minimum number of discontinuities in the system to avoid signal losses due to the mismatch of the excitation line with the 50Ω impedance set as characteristic impedance of the system. The electrical transmission line is represented by a micro-strip sketched in *Figure 4.10 (b)*, which is composed of a signal line made of copper, a substrate made of a particular material with high dielectric constant called Rogers 4003C, optimal to work in radiofrequency because it minimizes the power losses, and a ground plane.

The resonator is placed on the transmission line and the VNA measures the transmitted and reflected power, given as the parameters S_{11}, which is the power reflected back to port 1 with respect to the input power, S_{12}, which is the power transmitted to port 2 with respect to the input power, S_{21}, and S_{22}, that are the symmetric to the previous ones. A working resonator will allow us to detect a peak towards lower values of the S parameters in correspondence to the resonance frequency at which the device has been designed.

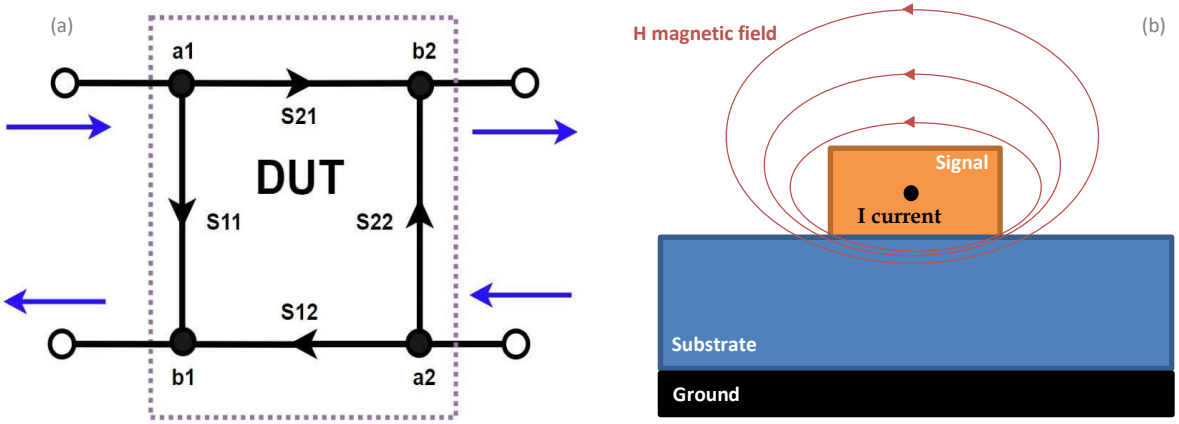

Figure 4.10: schematic of the DUT with the S parameters (a), schematic of the micro-strip (b).

4.6.1 Ring resonator design

The ring resonator we designed can be modeled as a series resistance-inductance-capacitance (RLC) equivalent circuit. The resonance frequency can be calculated as follows:

$$f_{res} = \frac{1}{2\pi\sqrt{LC}}, \quad (7)$$

Where C is the capacitance and is calculated as $C = \frac{\varepsilon A}{g}$, where A is the cross-section area, ε and g are the electric permittivity and the gap of the structure, and L is the inductance defined as $L = \frac{n^2 \mu \, Area}{h}$, where n is the number of loops made by the ring, μ is the magnetic permeability and h is the thickness of the structure[29]. For the calculations $\mu_r = 1$, supposing the material behaves as a dielectric, and $\varepsilon_r = 80$, considering the surrounding environment to be mostly water. The VNA is able to cover frequencies between 1 MHz and 6 GHz, so we defined the resonator geometry to obtain frequencies around 1 GHz. We chose this frequency because such value is easy to reach without having extremely large features or complex designs, so that the writing process is smoother and time saving. The calculations of the dimensions are done taking into account the substrate shrinking (see *Results* section, 5.2.3 *Writing resolution*), so the final frequency is foreseen considering a 40% shrinking of the final dimensions with respect to the one obtained after the writing. The final design is a ring as shown is *Figure 4.11 (a)*, where we tuned the radius, the width and the gap values to obtain the wanted resonance frequency.

Radius [mm]	**Width [μm]**	**Gap [μm]**	**Frequency** nominal	**Frequency** after shrinking
1	100	100	3 GHz	4.7 GHz
1.75	100	100	1.72 GHz	2.75 GHz
3	200	100	709 MHz	723 MHz

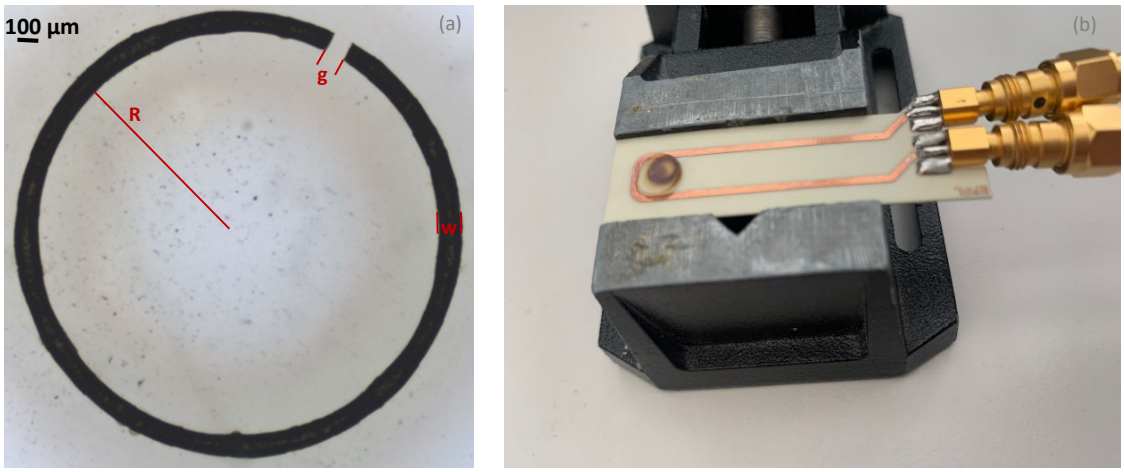

Figure 4.11: 1 mm radius ring resonator after writing (a), resonator embedded in gel during the testing on the microstrip (b).

5. Results and discussion

The majority of the results that are shown in this chapter refers to experiments made with hydrogels based on the DMAPS monomer. Some substrates are not suitable for the process and others have not been investigated for lack of time. The DMAPS based substrates revealed to be the most adaptable and easy to process from preliminary results, hence all the principal experiments make reference to this kind of hydrogels.

5.1 Substrate comparison

The substrates that have been selected for the experiments as described in section 4.*1* find their strength points in the easy processability, the biocompatibility and the different functional groups that can bind with silver ions. For each monomer we adopted an Edisonian approach to find a proper combination of monomer and crosslinker, before using the substrate for the direct laser writing experiments. The stiffness of the substrates should be included in the range that matches the one of the tissues for which our hydrogels could be used for. For instance an ideal range for the Young's modulus is between few kPa and a 100 kPa to operate in the range covered by soft tissues. For what concerns the strain at break we want to obtain at least a value of 15% to sustain physiological micro-movements, and at the same time we do not want the hydrogels to be too brittle because otherwise the samples can be easily damaged during the preparation for the writing process and even the formation of little cracks inside the matrix can compromise the final result. On the other side the hydrogel must have enough stiffness to sustain the printed structures and hold them together inside the matrix, so if the substrates can deform easily also the feature inside will be subjected to a change in shape that can affect the conductivity. Moreover the substrate must be optically transparent to not alter the efficiency of the laser at the 780 nm wavelength. To ensure these prerequisites we performed a tensile test on the different substrates and analyzed the results to select a feasible combination of monomer and crosslinker concentrations.

4.1.1 Mechanical characterization of hydrogel substrates

The first results from the mechanical test is done on the substrate made with DMAPS monomer. The final concentration of monomer we use for the experiment is 60 wt% with 0.6 mol% of MBAA crosslinker.

The *Figure 5.1* shows a strain at break around 70% and a maximum stress of 16 kPa, with similar values achieved for both the samples in water and in the PBS/glycerol solution. There is a little difference in the strain percentage between the samples soaked in the two liquids, indeed the presence of glycerol increases the viscosity of the solution with respect to pure water, and this factor can lead to a stiffer matrix, resulting in a lower strain. The difference overall is minimum, also because the glycerol is mixed with PBS so the swelling of the sample is not compromised by the high viscosity of glycerol and the resulting stiffening effect is not significant, and is probably balanced by the fact that glycerol also acts as plasticizer.

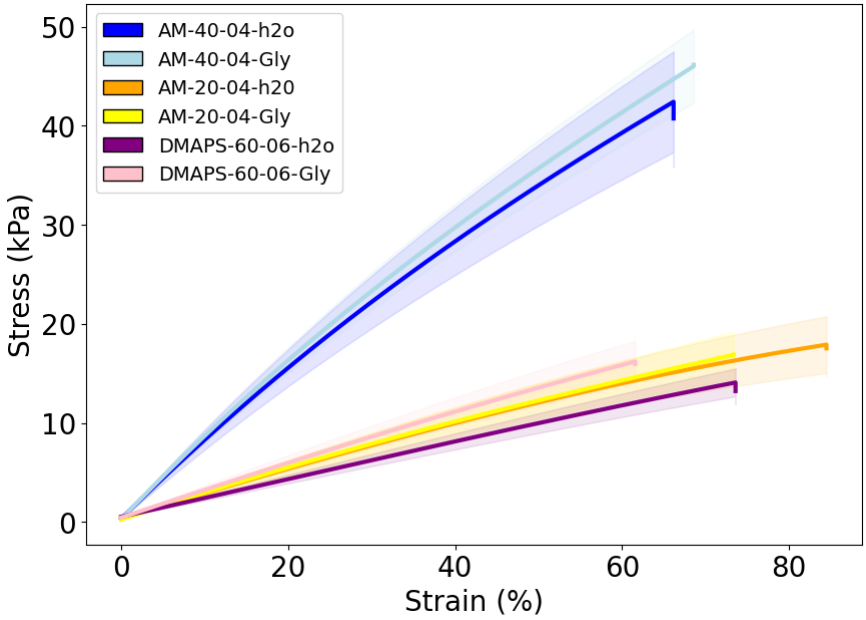

Figure 5.1: Stress Vs Strain curve for PDMAPS 60 wt%, 0.6 mol% MBAA, and PAM 40 wt%, 20 wt%, 0.4 mol% MBAA. Measurements done on n≥3 repetitions.

Hydrogels based on acrylamide monomer allow to have more freedom in tuning the monomer and crosslinker ratio, and still achieve a manageable substrate. We characterized two different hydrogels, one with 20 wt% and one with 40 wt% AM monomer, both with 0.4 mol% of crosslinker concentration. The substrate with 20 wt% monomer concentration has values for the stress and strain that are similar to the ones obtained for the DMAPS based hydrogel. This allow us to confront the writing process on substrates with similar mechanical properties, but based on different monomers, so the process is influenced directly by the characteristic of the molecule and not by the mechanics. The second monomer concentration of 40 wt% instead has the purpose to see if a different stiffness of the substrate can have an effect on the writing process, just changing the monomer concentration.

The acrylic acid samples are based on a 40 wt% monomer concentration and 0.6 mol% of crosslinker. Moreover a preliminary test has been performed by soaking the dog bones in the 1M AgNO3 aqueous solution to see the stiffening effect of the silver ions on the hydrogel substrate.

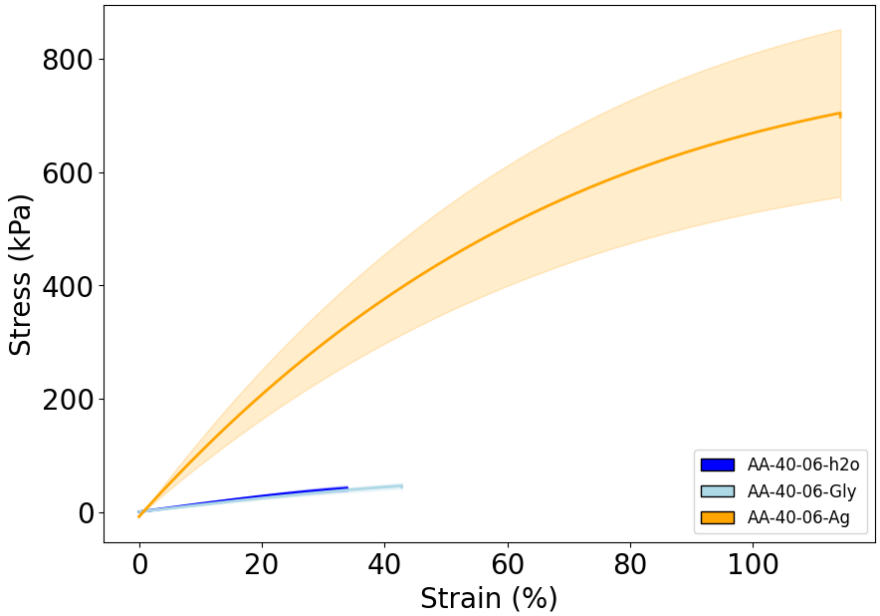

Figure 5.3: Stress Vs Strain curve for PAA 40 wt% with 0.4 mol% MBAA. Measurements done on n≥3 repetitions.

The curves for the substrates soaked in water and PBS/Glycerol solution show values for the stress and strain curves comparable with the ones obtained for the PDMAPS and PAM 20 wt%. The curve related to the substrate with the presence of silver ions shows instead a significant increase of the two parameters due to the strong binding of the carboxylic group with the silver ions that lead to mechanical reinforcement of the gel matrix due to metal coordination[30].

For the PAMPS substrates the tensile test has not been performed because the hydrogels based on this monomer have a high swelling ratio, and the swollen surface of the dog bones makes it difficult to perform a proper analysis on the samples. The characterization for this substrate relies only on the swelling ratio analysis reported in the paragraph *5.1.3.*

The Young's modulus is calculated from the previous curves, taking into consideration the slope of the linear region between the 0% and 15% of the strain. The PDMAPS and PAM 20 wt% present a similar Young's modulus respectively of 22 kPa and 26 kPa, as computed from *Figure 5.1* and *Figure 5.2*. The measured value is desirable for a possible final application that would involve a brain-like tissue, which has stiffness ranging from 1 kPa to tens of kilo Pascal. This result makes these two substrates the principal candidates to conduct the experiments from the mechanical point of view. The AM with 40 wt% monomer has a Young's

modulus which is five times higher than the first poly-acrylamide hydrogel, hence it is less compatible with the stiffness range previously mentioned, but it remains a valuable substrate to test the effect of the stiffness on the writing process. For all the samples the value of the Young's modulus is slightly higher in the case of soaking in the Glycerol/PBS solution, due to the effect of the viscosity of the solution with respect to water, but this is probably balanced by the plasticizer properties of the glycerol present between the polymer chains, which causes a reduction in the hydrogen bond between adjacent chains, leading to a less fragile substrate.

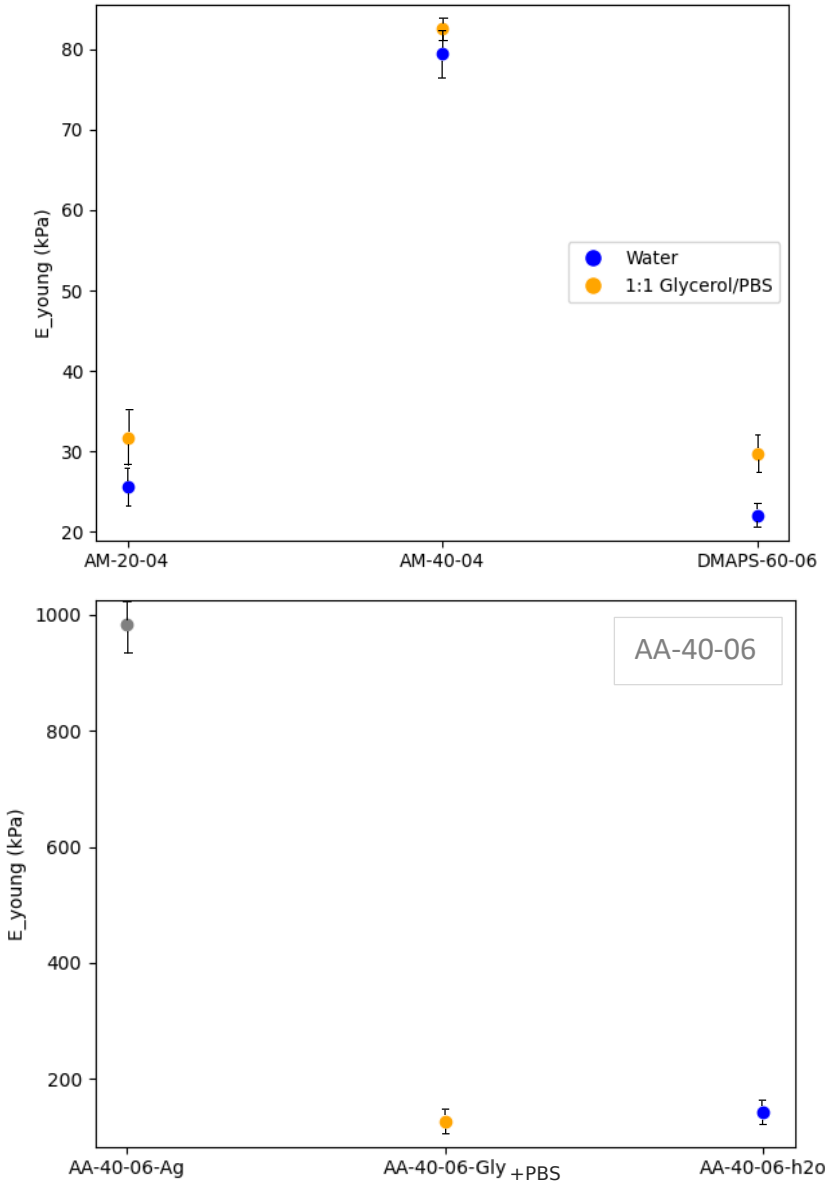

Figure 5.5: Young's modulus for PAA substrate. Measurements done on n≥3 repetitions

The poly-acrylic acid shows a significant stiffening of the matrix due to the silver ions, and the Young's modulus increases of nearly 100 times with respect to the

measurements performed on the samples soaked in water (see *Figure 5.5)*. This effect causes the substrate to become very brittle after the soaking in the silver nitrate aqueous solution, so it becomes impossible to handle the sample and prepare it for the direct laser writing process. This leads us to exclude the acrylic acid as a feasible monomer to use for the substrate preparation. The functional groups present in the different molecules at the base of the gel matrix play an important role in the decision of the substrates, and just from the mechanical characterization we can exclude the molecules with the presence of the carboxylic group in their polymeric chains, because the interaction with the silver is too strong and changes significantly the mechanical properties of the hydrogel.

5.1.3 Swelling ratio

The swelling ratio is analyzed to take into account the different media in which the substrates are soaked during the process, from the preparation of the hydrogel to the electrical measurement. Indeed the dimensions of the sample are strongly dependent from the liquid they are swelled into, and this factor can have an influence on the writing process. Also, we have to make sure that the content of silver ions is sufficiently high to ensure that the reduction process is not limited by the concentration of ions and the swelling analysis is useful to ensure that the substrates are at swelling equilibrium when we use them for the direct laser writing. From these analysis we established the minimum swelling time in the silver nitrate aqueous solution to be 48 hours, time after which a plateau is reached.

For the substrates based on PAM we have a similar trend for both diameter and mass as shown in *Figure 5.6*, and we reach the plateau already after 2 hours when soaking in water and PBS/glycerol solution, while in presence of the silver nitrate a constant value is reached around the 48 hours. The substrate with a 20 wt% monomer concentration has a higher swelling ratio, around the double with respect to the one with a larger presence of monomer. This behavior happens because when the gel matrix is formed, more polymer chains will form during the crosslinking process if more monomer is present, leading to a denser network that leaves a reduced number of free space within the matrix, limiting the amount of water that can be absorbed by the hydrogel. Also, the density of the chain causes the matrix to be more rigid, so when the water is incorporated, a more rigid network makes it harder to expand and stretch to accommodate the presence of the water molecules. The diameter analysis shows an inversed behavior of the substrates in the three solvents, so a larger dimension is reached for the water, while the minimum diameter corresponds to the soaking in the aqueous silver nitrate solution. Despite of this opposite trend the results are

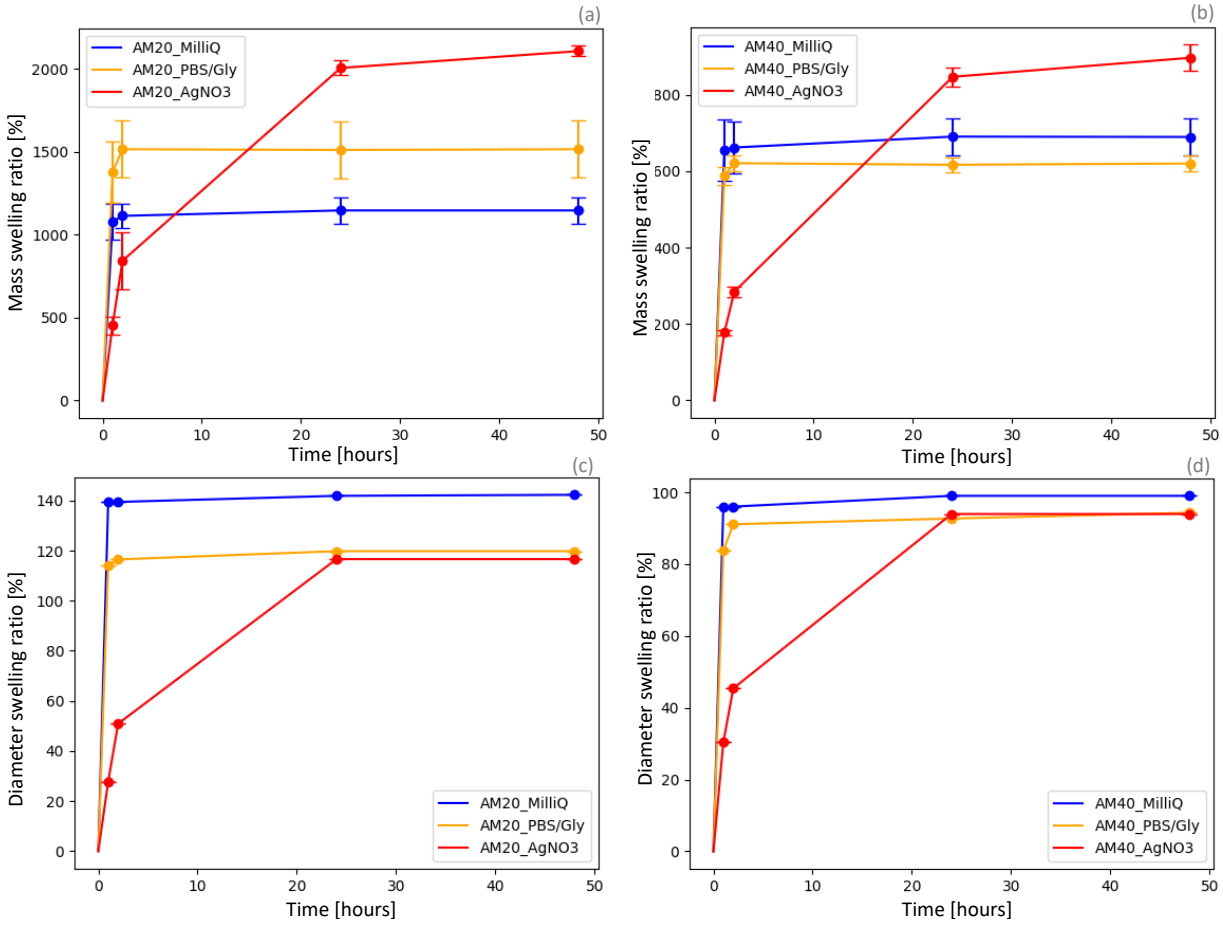

Figure 5.6: swelling ratio of PAM 20wt% monomer in the three solvents analyzed by mass (a) and diameter (c). Swelling ratio of PAM 40wt% monomer in the three solvents analyzed by mass (b) and diameter (d). Measurements done on n=3 repetitions

consistent, because an increase of dimension happens also in the thickness, because an increase of dimension happens also in the thickness, so overall the total change of volume is corresponding to the change in mass.

The PDMAPS substrate has a behavior similar to the PAM one, the principal difference between the two is that the PDMAPS swells around 7 times more in the silver nitrate aqueous solution than in the other two solvents, while this difference is much less evident for the PAM, where the swelling variation is less than two times. As a consequence, we observe a diameter that is three times larger with the silver ions than in the PBS/glycerol solution, so after the writing process we have a consistent shrinking of the samples when we perform the electrical measurements with respect to the initial condition. This factor can influence the geometry of the written features, so we must pay attention to the behavior of the metallic structure after the rinsing of the samples in water, to control if the shrinking actually affects the tracks.

For what concerns the PAMPS substrates, the trend is opposite to the ones already described both for mass and diameter, so we see the maximum swelling

ratio when the substrate is soaked in water, while when the silver nitrate is present in the solution we have a minimum in the swelling. The diameter behavior indicates that we have a sample that is three times larger in the PBS/glycerol solution compared to the initial condition, so the structures are influenced in the exact reversed way with respect to the PDAMPS samples. If the tracks follow the change in size of the substrates, the swelling factor can be a key point for the choice of the monomer on which the hydrogel is based upon, because a high swelling can lead to an enlargement of the silver structures and destroy the percolation, while a shrinking of the substrate may actually help the nanoparticle clusters to make contact between each other and help the percolation.

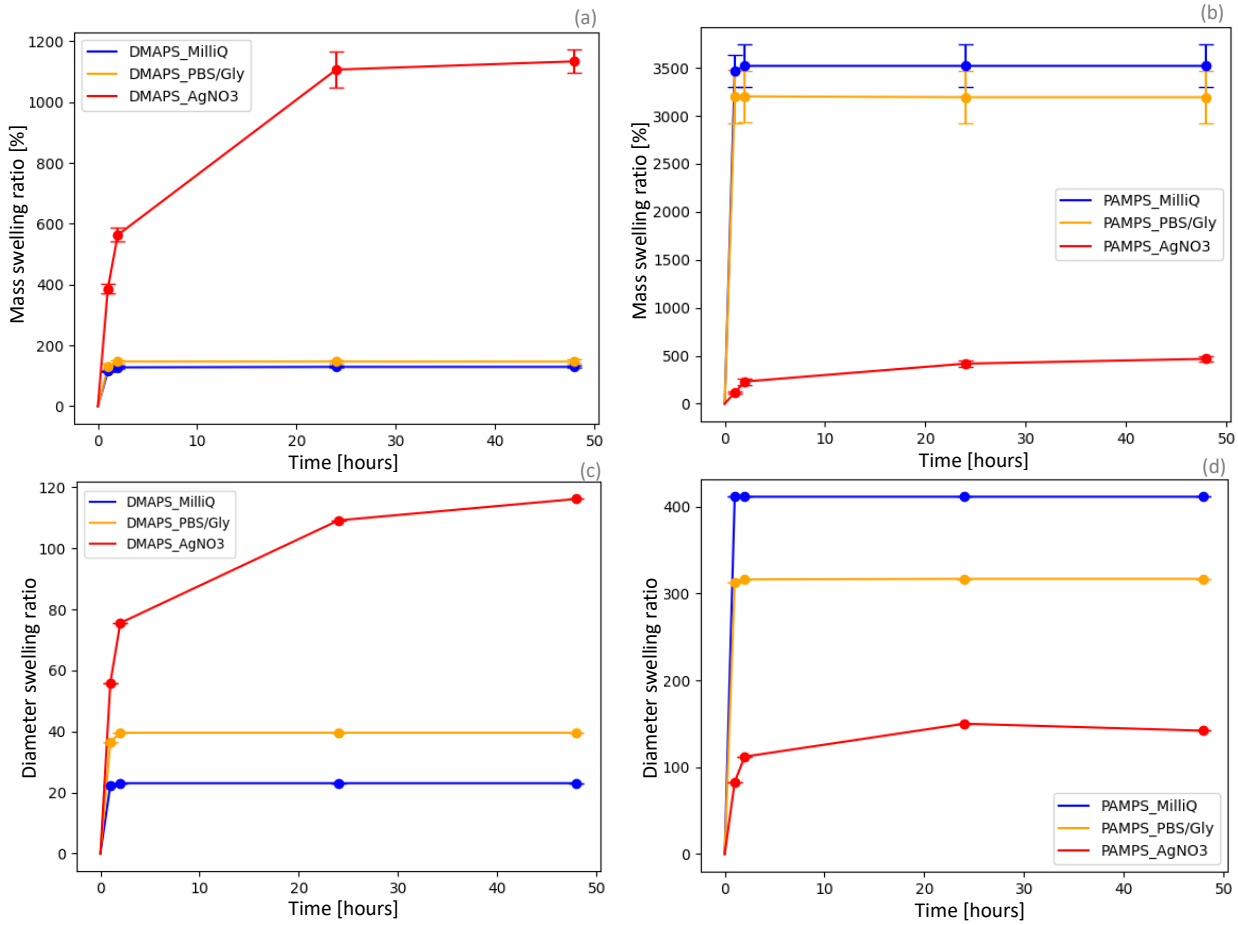

Figure 5.7: swelling ratio of PDMAPS in the three solvents analyzed by mass (a) and diameter (c). Swelling ratio of PAMPS in the three solvents analyzed by mass (b) and diameter (d). Measurements done on n=3 repetitions

5.2 Writing parameters and characterization

The design of the structures we want to embed inside the gel matrix is thought to have a simple geometry that allows to facilitate the electrical measurements performed with the probe station. The objective is to obtain a structure where we can achieve the percolation of the silver nanoparticles that form during the writing, and to do so we have to combine a good design with the optimum choice of writing parameters that can give us a final conductive structure. The structures inside the hydrogel are written at a distance from the gel surface of 50 µm. This limit is due to the presence of the glass on which the sample is placed to perform the writing. When the laser is scanning through the hydrogel, bubbles form coming from the boiling of the water present inside the matrix. These bubbles tend to escape towards the surface of the gel and when they encounter the glass interface, the air is trapped between the hydrogel and the glass. When this happens the initial position of the sample on the z-axis is shifted, so the machine loses the focus of the interface and the effect of the laser is canceled by this layer of air and water that damages the adhesion between substrate and glass. On the other hand, the upper limit is set by the objective working distance which prevents us to write features at z-values higher than 190 um.

5.2.1 Parameters selection

The writing parameters have been determined by doing a series of experiments on the surface coverage of a square matrix 3x3, of side 100 µm long and 5 µm thickness (see *Figure 5.10*). The different parameters, i.e. hatching and slicing distance, laser power and scan speed are tuned one at a time, to see if is possible to recognize a trend on the area coverage of the written square with silver nanoparticles that follows the change of the single parameter. For the hatching and slicing distance the results are taken from the previous results. Previous preliminary results show that for the slicing distance is ideal to use a value that allows the interpolation of the laser voxel in subsequent layers, where 1 represents the minimum distance for which the laser scan do not overlap between two layers. With a slicing distance lower than 1, the results show that the area coverage is independent from the hatching distance when a certain number of layers is reached. Based on these results, in order to save writing time, a slicing distance of 0.7 um and a hatching distance of 1 um are selected as writing parameters. Furthermore an offset of the hatching angle of 90° is added to writing parameters, so the scans will be performed for each layer with a different

direction, so that the scan lines can superimpose more with each other and help to have a better coverage, as shown in *Figure* 5.9 *(a)*.

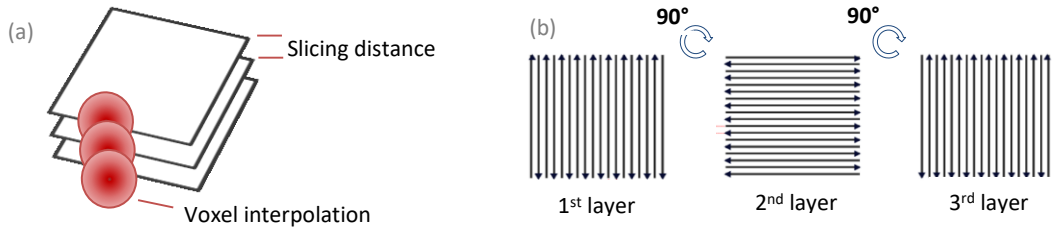

Figure 5.9: schematic of the laser interpolation over subsequent layers (a) and laser scanning path with hatching angle offset (b).

To select the laser power and scan speed, we fixed the slicing and hatching distances at 0.7 µm and 1 µm and used a laser power of 10%, 40%, 70%, and 100%. The scan speed was varied from 5000 µm/s to 100000 µm/s.

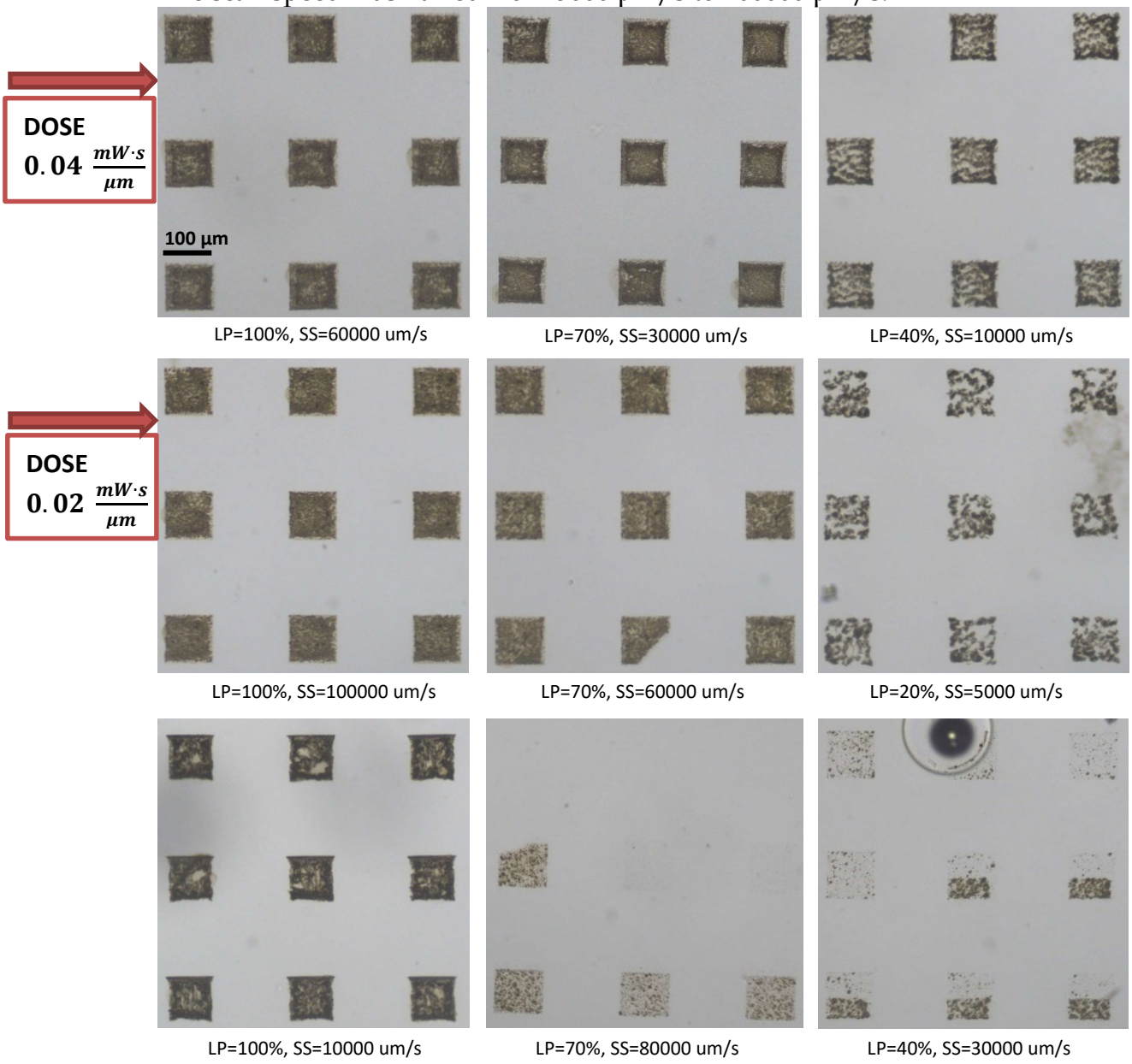

Figure 5.10: printed silver matrix for laser power and scan speed analysis.

The effect of laser power and scan speed combination was quantified by measuring the area coverage.

First, we used different combinations of scan speed and laser power to obtain the same dose value, calculated as defined in paragraph *4.3.2*. For different doses values we notice a constant trend of the area coverage with respect to the laser power, as shown in *Figure 5.11* the higher the laser power, for the same dose value, the higher the coverage. This behavior can be due to the fact that, even if the dose is the same and so we have the same amount of energy per second over a micrometer, a higher laser power might help to reach more easily the nucleation threshold, leading to an enhanced seeding that results consequently in a better area coverage. The role of the particle seeding is well illustrate in the work of Freyman and Waller, where they show how the particles grown into agglomerates starting from the initial layer made of the nucleated ions, which are called seeds[22]. When keeping constant the laser power and varying the scan

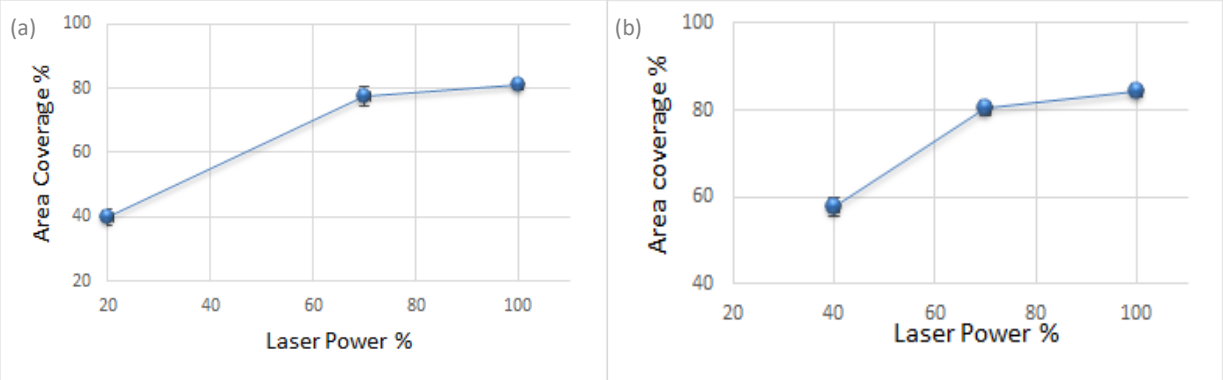

Figure 5.11: Area coverage percentage depending on the laser power for constant dose value: 0.04mW· s· µm^{-1} (a) and 0.02mW· s· µm^{-1} (b).

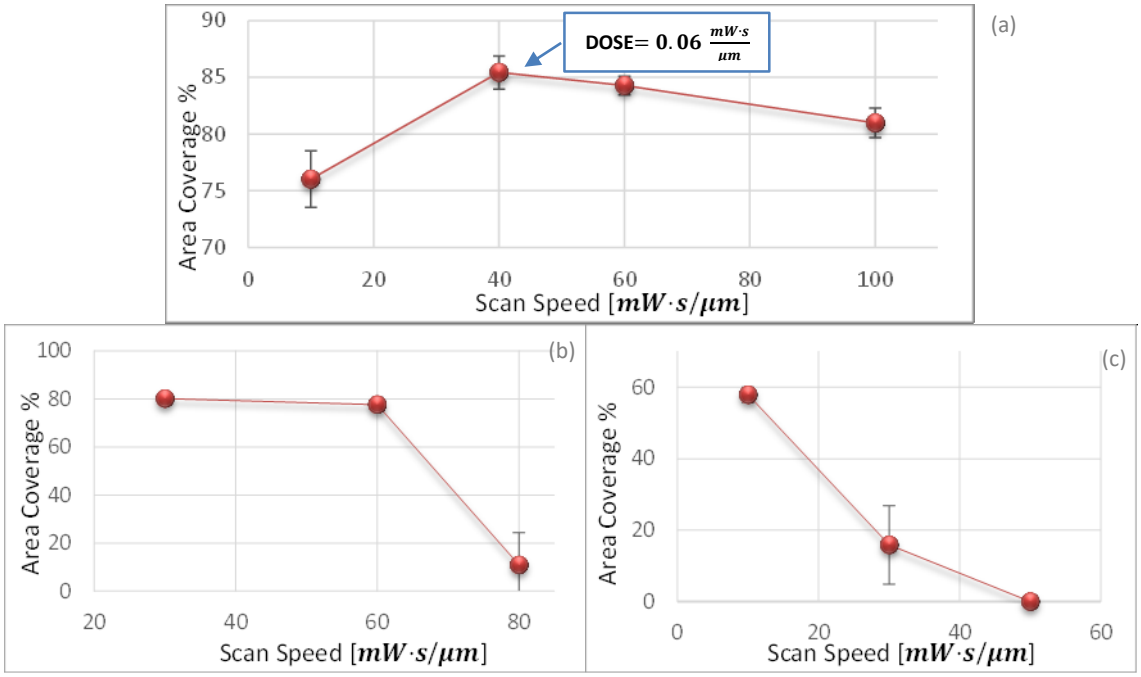

Figure 5.12: Area coverage percentage depending on the scan speed for a fixed value of the laser power: 100% (a), 70% (b), and 40% (c). Measurements done on n=9 repetitions.

speed, the coverage has always a maximum that is found for values that gives a dose quantity close to 0.06 $mW \cdot s \cdot \mu m^{-1}$.
Combining these two results, we found an optimum combination of values for a laser power of 100% and scan speed of 40000 µm/s, that allow us to have a better area coverage with a quite elevated scan speed, which is a good requirement to save time during the writing process. Moreover, from the graph referring to laser power of 40% and scan speed of 50000µm/s in *Figure 5.12 (c)*, we can extrapolate a dose threshold value of 0.01$mW \cdot s \cdot \mu m^{-1}$ below which no nucleation of silver nanoparticles is visible on the substrate. This indicates that for the combinations of scan speed and laser power that do not exceed this dose quantity, the energy provided by the laser is not sufficient to trigger the reduction of the silver ions, and consequently the nucleation and growth process cannot take place. Even if we can define an experimental way to select the best combination of laser power and scan speed, the two parameters are strongly dependent on the structure to write and on the substrate on which the direct laser writing is performed. Moreover an ulterior factor to consider is the bubbling effect that inevitably happens due to the thermal effect generated by the laser energy. This effect tend to increase with higher intensities and is one of the main reasons why keeping the dose value constant while changing scan speed and laser power, does not guarantee to achieve the same writing quality of the structures for the same dose. The parameters defined in this section are optimized for substrates made with the DMAPS monomer, hence if the hydrogel used is different it might be necessary to perform a similar analysis to select the most suitable parameters.

5.2.2 Tracks design

The first design we implemented is a simple track of 5 µm thickness and a length of 1 mm, with two squared pads of 200 µm side at the extremities placed to facilitate the contact of the track with the tips of the probe station.
Through a visual analysis with the inverted microscope incorporated in the Nanoscribe machine, from the images taken in reflection mode (*Figure 5.13 (b)*), we can appreciate a percolation of the silver particles composing the tracks that form a potentially conductive structure. However, when we try to perform the electrical measurements on the structures, we do not see a significant difference between the conductivity of the gel matrix alone and the one of the tracks. When we measure the features, the equipment do not allow us to have a control of the depth of the tips that are going through the hydrogel substrate and therefore we have to breach into the metal structures to be sure that we reached the 50 µm depth where we can find the contact with the track. Hence, being the approach with the probe tips partially destructive, one hypothesis to justify the result is

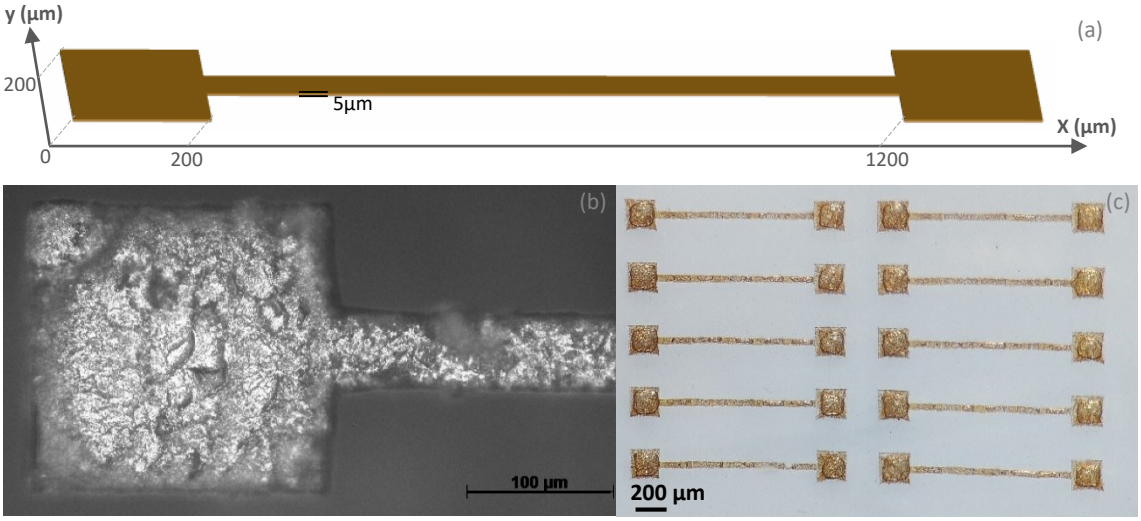

Figure 5.13: track and pads design (a), inverted microscope image of the pad taken in reflection (b), image of the tracks and pads takes with the stereomicroscope (c).

that the structures are too delicate and the contact with the tips actually interrupts the percolation because it damages the tracks. A second and more probable option, is that the silver agglomerates are not dense enough to provide a conductive path along the entire design, but they are interrupted by some voids due to the bubbles formation during the writing and so the percolation is present just in isolated points of the track. To solve these problems we thought about increasing the thickness of the structures from 5 um up to 40 µm. Indeed, with a thicker structure the probes have a larger contact area also in the z-direction and increasing the number of layers composing the track we improve the chance to have a conductive path, achieving an overall percolation between the layers that can overcome the interruptions caused by the bubbles. Also in this case, we can appreciate percolation of the silver agglomerates on the last layer, formed after the nucleation process. The silver nanoparticles are clearly localized to the design area, as visible in *Figure 5.14 (c)*, so the gel remains transparent and the reduction process happens only where the laser scans the substrate. This gives us a resolution of the features after the writing process that has a maximum deviation of 3% for the length, while for the width we have a maximum deviation of 16% from the theoretical value. Electrical measurement on the thick tracks design revealed a significant increase in electrical conductivity, so the experiments for the conductivity measurements have been implemented based on this structure. The 100 µm width and the thickness are kept constant for all experiments, while the length is the only parameter that changes. We conducted the experiments on tracks of 1.5 mm, 2 mm, 3 mm and 4 mm and to make the process more autonomous we designed the tracks into arrays of multiple tracks, so that the writing process has not to be started manually for each single feature. The combination of parameters that we selected in the previous section allow us to

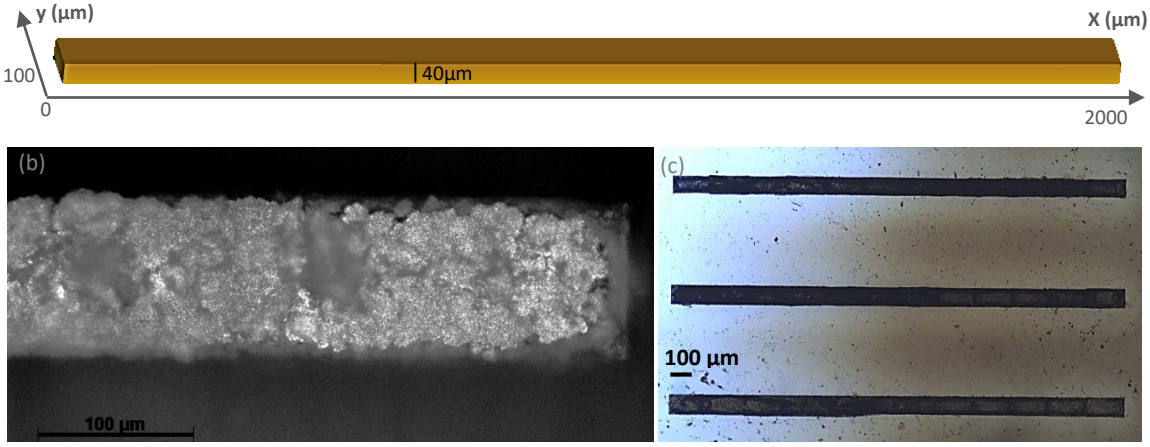

Figure 5.14: thick track design (a), image of an array of 3mm long tracks taken after writing with the optical microscope (b), image of track portion taken with the inverted microscope in reflection (c).

get an eight tracks array in a time between one and two hours depending on the length, which can be considered a reasonable process time for the method used.

(a)

5.2.3 Writing resolution

During the writing process, the silver nanoparticles nucleate in a localized way, providing features that corresponds to the theoretical design from the software. However, after the writing, the substrates are soaked first in water and then in the PBS/glycerol solution and this causes the hydrogels to shrink or swell, based on the solvent they are swelled into. To analyze the electrical results we need the value of the length and thickness of the structures at the moment of the measurements. Moreover, we want to investigate the dependency of tracks shape and conductivity on the swelling behavior of the substrate. Hence, we quantified the writing resolution of the features by doing an optical analysis of the track dimensions in the three phases of the process, i.e. after the writing with the substrates soaked in the 1:1 water/glycerol silver nitrate solution, after the rinsing in water, and lastly in the 1:1 PBS/glycerol solution. Accordingly with the results of the swelling ratio for the substrates based on the radius measurement in the paragraph 5.*1.3*, the tracks change their size following the shrinking of the hydrogel in the different liquids. After the writing process, the resolution is better for the length, because it is one order of magnitude larger than the width. The larger scale reduces the impact of variability in the laser's precision, making the resolution less sensitive to minor fluctuations and inconsistencies that have a more pronounced effect on smaller features like the width.. Another factor that affects the resolution is due to the writing of thick structures, indeed the growth of the particles over subsequent layers tends to

partially enlarge the structure and also a minimum offset of the laser with respect to the previous layer is present when moving on the z-axis, enlarging the width.

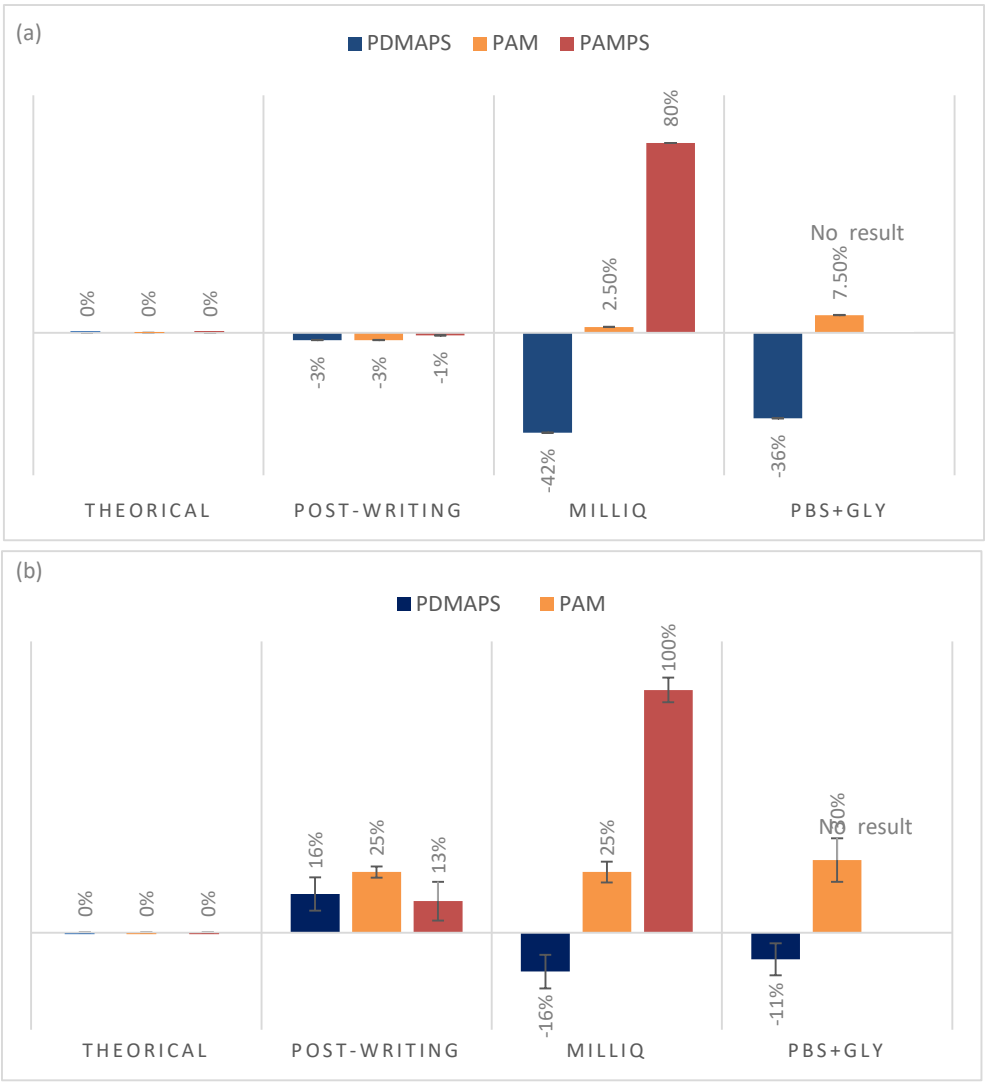

Figure 5.15: writing resolution of the silver tracks for the length (a) and the width (b).). Measurements done on n≥16 repetitions.

The values for the length that we obtain post-writing are almost equal to the ones of the theoretical design, while for the width, as previously specified, we have a slight increase of the dimensions. However, the factor that interests us the most is the change of the dimensions between the different solvents. Indeed, we notice two main trends from post writing to the final environment. Firstly, the one followed by the PDMAPS evidences a shrinking of 36% of the length in the PBS/glycerol solution with respect to the theoretical value as calculated in *Figure 5.15 (a)*, and a shrinking around 11% for the width (*Figure 5.15 (b)*). On the other hand, the PAM and PAMPS substrates behave in the opposite way, so we have a positive size increase for both length and width compared to the theoretical one. This happens accordingly to the swelling behavior of the radius, by the time PAM

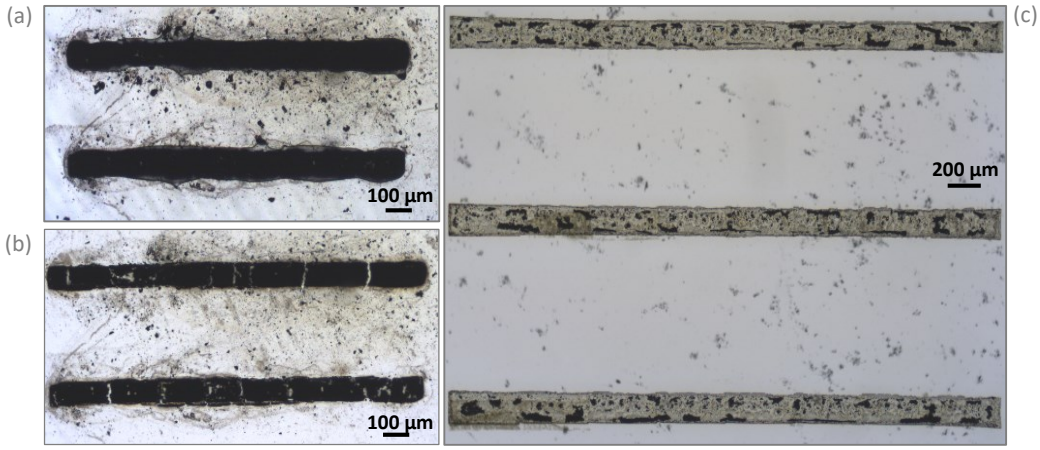

Figure 5.16: tracks in PAM after writing (a), discontinuous tracks in PAM in water (b), tracks in PAMPS in water without percolation (c).

and PAMPS swell more in water and the PBS/glycerol solution than in the aqueous silver nitrate solution, and as a consequence also the silver tracks embedded in the gel follow the same trend. From this result, we realized that substrates that behave like the PAMPS and swell a lot in water, represent a problem for the metal structures. When the structure size increases because of the swelling, the nanoparticles agglomerates are torn apart and the percolated structure is totally destroyed. In *Figure 5.16 (c)* we can see how in water the tracks are not anymore continuous as after the writing, but the "black spots" that represent the silver particles are dispersed into a larger structure and do not percolate anymore. This problem is less visible for the PAM because the swelling is very similar between PBS/glycerol and the silver nitrate aqueous solution, but still we can notice some voids forming throughout the tracks that compromise the percolation, and as a consequence do not allow us to measure a value for the conductivity. Even if parameters optimization has not been further investigated for the PAM substrates a first conclusion is that substrates that swell more in the PBS/glycerol solution then when the silver ions are present, might not be suitable for our process because they compromise the continuity of the structures after the writing.

From these last results we exclude for now the use of substrates that have a higher swelling ratio in water and PBS/glycerol with respect to the silver nitrate aqueous solution, like the PAMPS and PAM. based on the analysis made on the substrates, the PDMAPS seems to be the best candidate to be used as base for the direct laser writing. Moreover, we have a high consistency between the values we obtain for the final dimensions for different tracks. Indeed, for all the measured tracks of the different lengths we obtain a constant shrinking of 36% with respect to the theoretical design for the length and around 10% for the width. This allow us to have a precise control on the geometry of the structures we want to obtain, so if there is the necessity to design a feature that has to fulfill

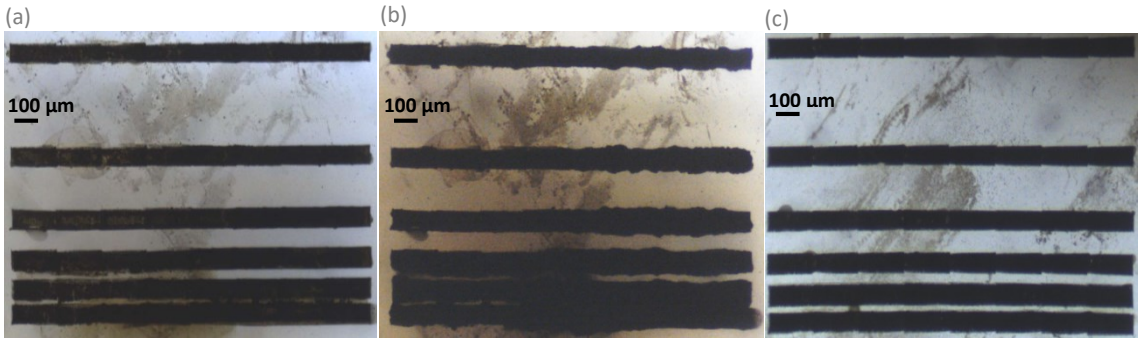

Figure 5.17: pitch resolution test for distances of 25um, 50um, 100um, 200um and 400um. Tracks of 40um thickness after writing (a) and after water rinsing (b), tracks of 5um thickness after rinsing (c).

dimensional requirements we can compensate the final shrinking by adjusting the initial dimensions of the design and obtain in the end the wanted geometry even for more complex features. While making a project of a structure we want to write, we also have to take some precautions due to the shrinking. Indeed not only the features undergo a dimension reduction but of course also the distances between them. In *Figure 5.17 (a)* and *(b)* we can see how the pitch resolution changes between the post-writing phase and the soaking in water. For thicker structures we still see a spacing between the features at 50 µm when the silver nitrate is present, while after the rinsing in water the adjacent structures are touching each other for the same value. Hence a reasonable design distance between two features is around 100 µm when writing thick structures, to ensure we do not have an overlap afterwards. If thinner structures around 5 µm are made, as in *Figure 5.17 (c)*, the pitch resolution can reach a lower value of 25 µm. For lower thicknesses the geometry is not deformed by the formation of superficial bubbles and the misalignment of the laser between the layers is not present, so the absence of the enlargement effect due to these two phenomena allow to reach lower spacing between the features.

5.2.4 Micro-CT analysis

To characterize the resistivity we obtain from the electrical measurements, the last parameter we need is the thickness. After the analysis on the 2D geometry of the samples we expect a dependency on the shrinking also for what concerns the thickness of the tracks. To evaluate it we performed a Micro-CT on the silver tracks and tried to extrapolate the measure from the 3D reconstruction.
In *Figure 5.18 (c)*, we can notice how the tracks are being deformed due to the shrinking effect of the substrate, so we do not obtain a linear structure, but along the z-axis the track is folded and we do not appreciate a uniform rectangular structure as the one from design. This shape makes it difficult to distinguish between the parts where the track is twisted or overlapped and the actual

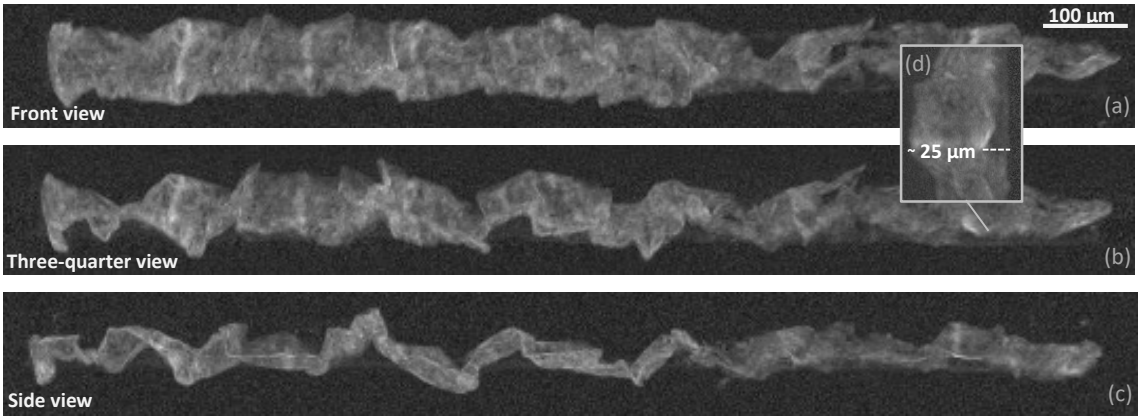

Figure 5.18: 3-D reconstruction of a 2 mm silver track with the Micro-CT imaging. Front view (a), three-quarter view (b), side view (c) and zoom-in on the track thickness (d).

projection of the z-axis, so it is complicated to obtain a precise measure of the thickness. Moreover, along the majority of the track, we can only distinguish the silver track as a thin layer present on the surface of the 40 µm thickness, while the remaining part is just visible as a shadow below the first layer. A possible explanation to this outcome is that an actual percolated structure forms during the writing of the last layers of the track, growing above the particle seeds that nucleated during the first scans, while along the rest of the thickness some nanoparticles are present but they do not form a dense network. During the Micro-CT scan, the conductive metal part absorbs the most of the X-rays, while the other part of the structure is not dense enough and lets some X-rays passing through the voids that are filled with the gel matrix and water, so the light reaches the denser layer placed behind and is absorbed again in the same plane. Consequently, in the 3D reconstruction only the percolated part is defined, while the remaining thickness is barely visible as a shadow in the back. Considering the difficulty in selecting a non-arbitrary defined zone to be considered as the real thickness, we can estimate an overall value for the thickness between 20 µm and 35 µm. Considering that the size change of the length is consistent with the diameter shrinking of the substrate, we can expect a similar behavior for the thickness of the tracks with respect to the shrinking on thickness of the substrate. Following this reasoning, a value around 20 µm for the tracks is coherent with the swelling analysis performed on the thickness when the PDMAPS substrate is soaked in the three solvents used throughout the process. Indeed the difference between the silver nitrate aqueous solution and the PBS/glycerol solution is about 50%, so we can expect an analogous shrinkage of the structure thickness. The value indicated for the thickness is anyway indicative and cannot be considered as an exact reference value for the characterization. Another problem that emerges is that from the reconstruction of the track only a 5 µm layer shows an evident percolation, so the results coming from the electrical measurements

are actually referred to a track that probably is not even 20 µm but one order of magnitude lower. The cross-section value then is different if we consider only the dimensions of the conductive part we are measuring or if we also include the shadowed area that is not contributing to the electrical results. Even if the used imaging technique did not help us getting to a consistent conclusion about the thickness of the tracks, is still a resourceful technique to prove the existence of a percolation within our structures. Indeed the frontal view of the structure allows to appreciate a continuous layer of silver along the entire length of the track that indicates the actual percolation of the reduced silver ions after the nucleation and growth process occurring during the writing, and it allows to visually justify the conductivity measured on those kind of features.

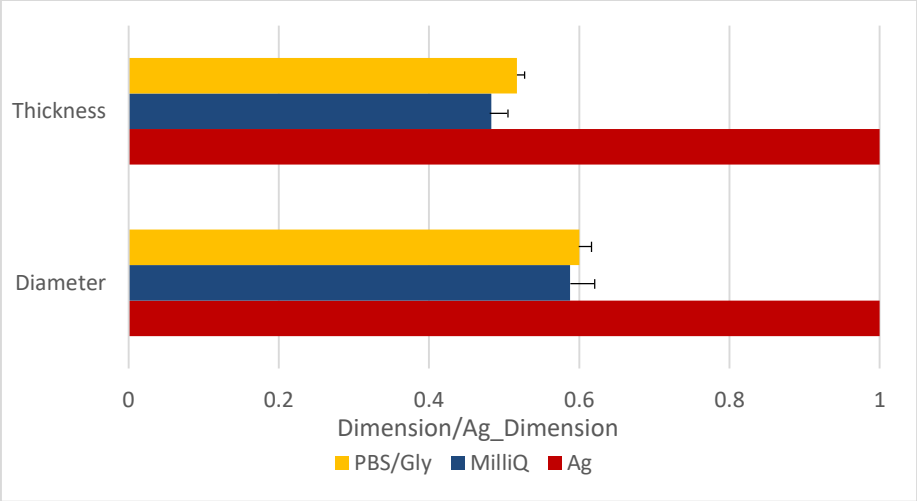

Figure 5.19: dimensional analysis on the diameter and thickness of the substrate depending on the liquid environment, normalized with respect to the dimensions in the silver nitrate aqueous solution. Measurements done on n=3 repetitions.

5.3 Electrical characterization

The first attempt of electrical measurement was done on the thinner tracks, but no difference with the characteristic I-V curve of the gel matrix was found. The final conductivity measurements are performed on the second track design with dimensions of 100 µm width, 40 µm thickness and variable lengths of 1.5 mm, 2 mm, 3 mm and 4 mm. The measurements on the thick tracks show the typical behavior of an ohmic conductor, which it is the silver indeed, and we can clearly appreciate the difference between the conductivity of the track with respect to the hydrogel matrix. The measurements on the matrix without the presence of the silver show a maximum value for the current around 10 nA, while the silver tracks reach a peak of 2.75 mA, that is the maximum value we can measure due to a saturation limit of the instrument.

This result evidences a difference in resistance of six orders of magnitude between the hydrogel and the silver tracks, which reveal to be indeed conductive. The setup used to perform the measurements is not optimized for non-rigid samples and moreover do not allow us to have a good focus on the features inside the substrate, so we performed further characterizations to confirm that the results we obtain are actually due to an electrical conductivity of the tracks and not, for example, by the contact between the tips underneath the hydrogel.

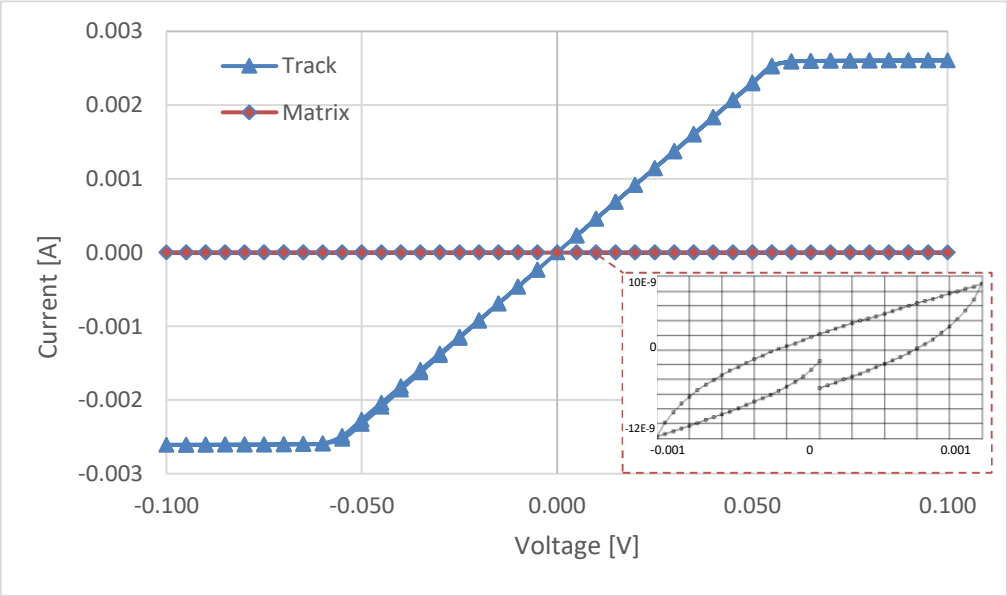

Figure 5.20: I-V curve comparison between the conductive track and the hydrogel matrix.

5.3.1 Stability of the two-probe measurement

Firstly, we performed repeated measurements on the same track, without changing the position of the probes between the consecutive acquisitions. In *Figure 5.21* we can see how the values of the resistance are randomly placed around a mean value and do not follow any particular trend. Indeed, an increase of the resistance from a measure to the next one, it would suggest that either the silver structure is progressively damaged by the tips during the measurements leading to a reduced percolation and consequently to a higher resistance, or that some electrochemical reactions are happening due to the applied voltage that influence the stability of the track conductivity. In our case the value is repeatable and the variation with respect to the mean value is less than 2 Ω, and is mainly due to the fact that the hydrogel is a non-rigid substrate, so the substrate is still able to relax around the probes and slightly change the contact position after the tips are placed in contact with the tracks, which causes a little instability of the measurement that is anyways negligible for our purpose.

(a)

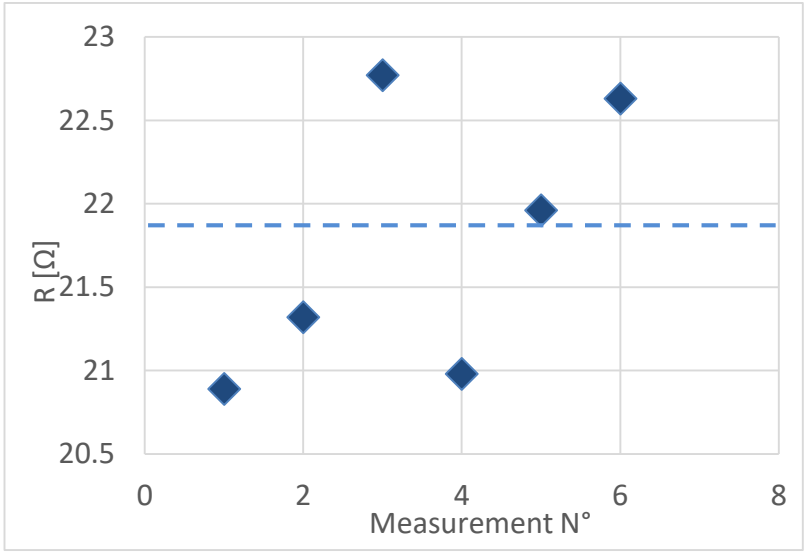

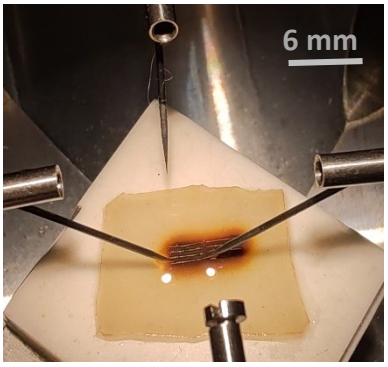

Figure 5.21: randomness of the resistance value for consecutive measurements on the same track (a), tracks embedded in the hydrogel during the measuring process (b).

5.3.2 Dependency of electrical resistance on tracks length

Following Ohm's law, the resistance in a uniform conductive material is directly proportional to the length of the conductor. We fabricated tracks with different lengths to confirm that the silver tracks are behaving experimentally as expected from a metallic conductor material and the results are not driven or modified by other phenomena. In *Figure 5.22 (a)* we appreciate the slope change that decreases from the 1.5 mm tracks, to the 4 mm ones, suggesting an increase of the resistance with the length.

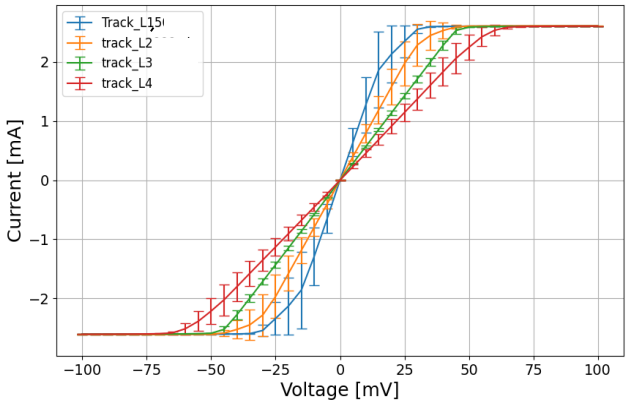

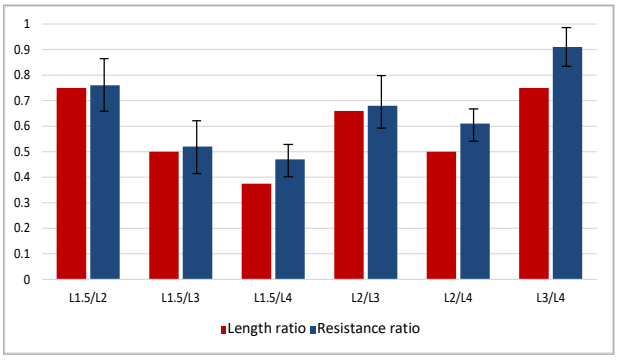

Figure 5.22: current Vs voltage curve for track with length of 1.5 mm, 2 mm, 3 mm and 4 mm performed on n≥3 repetitions for each track (a). Comparison between the length ratio and resistance ratio measured on the corresponding tracks (b).

In *Figure* 5.22 *(b)* we calculated the ratio of the measured resistance between the different lengths and compared the results with the corresponding length ratio of the tracks. For lengths of 1.5 mm, 2 mm and 3 mm the relationship between the resistance values differs only of a maximum of 3% from the nominal ratio

Length [mm]	R [Ω]	ρ [Ω·m]
1.5	11.80	$4.13 \cdot e^{-5}$
2	15.44	$4.05 \cdot e^{-5}$
3	22.78	$3.99 \cdot e^{-5}$
4	25.03	$3.29 \cdot e^{-5}$

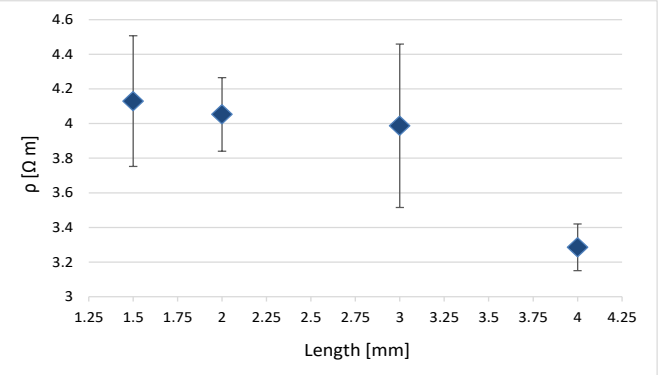

Figure 5.23: table with the measured values of resistance and resistivity for different track lengths and graph of the resistivity depending on the length. The resistivity value has been calculated on an average of n = 6 tracks per length.

between the lengths. Where the 4 mm tracks are involved in the calculation, a deviation of about 20% from the theoretical value is present, but we can still consider the result to be significant to justify a conductor like behavior of the tracks. Indeed, we have to consider that the contribution of the contact resistance is not removed from the measurements and it can influence the accuracy of the results, especially for the cases where the resistance is lower because the contact resistance represents a larger fraction of the final value with respect to a more resistive structure. So, it is possible that for the shorter tracks the effect of the contact resistance is similar and the final ratio removes its influence resulting in an almost perfect equivalence with the length. For tracks of 4 mm the effect of the contact resistance can start to be less impactful, leading to a larger error that is not totally compensated when we perform the ratio between the different tracks. However, as previously mentioned, the accuracy of the results is still strongly influenced by the setup that is not optimized to perform measurements on hydrogels substrates, so the values can undergo a significant change even when millimetric displacements of the tips are done, hence the justifications for the obtained results are not based on any experimental proof.

From the calculated resistance values we can quantify the resistivity of the tracks and accordingly to the theory, we get a constant value for all the tracks, as it is independent from the length. As a consequence to the non-exact proportionality of the resistance to the length, the resistivity corresponding to the 4 mm track differs of 20% in average from the one characterizing the other tracks. The resistivity is calculated considering the actual length and width that structures assume after the shrinking process when they are stored in the PBS/glycerol solution, as described in section *5.2.3*. The thickness considered in this case is 35 µm estimated with the Micro-CT imaging, considering the worst case value for the thickness. If we make reference to the 3D reconstruction of the tracks, only a layer of about 5 µm seems to have a percolation that can give conductivity. To calculate the resistivity we could also consider this measure for the thickness,

considering only the part of the track that actually is conductive, instead of taking in consideration the whole structure. In this case we would obtain a resistivity that is one order of magnitude lower than the one showed in *Figure 5.23.* Overall, in the worst case scenario we obtain a resistivity on the order of 10^{-5} Ωm that compared to the bulk silver is still three order of magnitude higher, but to get close to the value of the bulk silver of 10^{-8} Ωm it would require a larger study on the used methods and materials, to try to limit the voids and defects caused by the bubble effect and the irregularity of the writing. Even if the resistivity is quite large if compared to the bulk silver, if we compare our results to the ones found in literature we find a correspondence with the values obtained by the groups of Stellacci[24] and Waller[26], which performed measurements on silver structures in presence of a surrounding polymer reaching the same order of magnitude we got for the resistivity.

5.3.3 Resistance stability over time

The electrical measurements performed on the tracks are done through a quite destructive method. To get the contact with the metal we have to make the tips passing through the structure, and this maneuver inevitably damages the track around the contact point. To test the stability over time, we measured again the tracks one month and two months after the first attempt, and overall we were able to obtain a new result on the 80% of the tracks. This shows that the structures can withstand some limited intrusions that can break the layers and still be able to maintain the percolation. The hydrogel matrix is able to deform when the tips enter inside the sample to reach the tracks, and when they are removed after the measurement the hydrogel goes back to its original position, probably helping the silver particles to rejoin together in the point where the tip was placed, partially reducing the damage. From the repetitions, we calculated again the values of the resistance for the different tracks, to verify if the storage time has any effect on the silver structures. Indeed the samples are stored inside the PBS/glycerol solution, so the presence of water in the environment could affect the conservation of the tracks. Some oxidation or degradation processes can actually take place in time and modify the conductive properties of the silver that would lead to an increase of the measured resistance.
In *Figure 5.24* we can see that the resistance is overall stable in time, and the change of the values do not follow an increasing trend. The main factor contributing to the differences between the repetitions is due to the measuring method, indeed the quantity of current passing through the tracks changes depending on the position of the tips. So a variation of few Ohm is justified by

the inevitable modification of the contact point between the successive measurements. Indeed the silver structures are not perfect, and the positioning of the tips allows to find different conductive paths that, depending on the quantity of defects present on the way to the opposite extremity, can be more or less resistive.

Up to this point the direct laser writing process allows us to obtain structures directly embedded into the hydrogel substrate without further processing, and the tracks we were able to analyze show a conductivity in the range from 10^{-6} S·m to 10^{-5} S·m that is comparable to similar methods found in the literature where a value of 10^{-6} S·m was reached[22]. Moreover the structures present a high stability in time, with a maximum variability of the resistance of 16% after 60 days from the first measurement. The electrical measurements have a high reproducibility with a variability of the resistance below 10% between structures with the same geometrical and writing parameters, both in time and between distinct samples. From this starting point the process can be used to obtain geometries different from the simple tracks, and realize more complex designs depending on the user necessities.

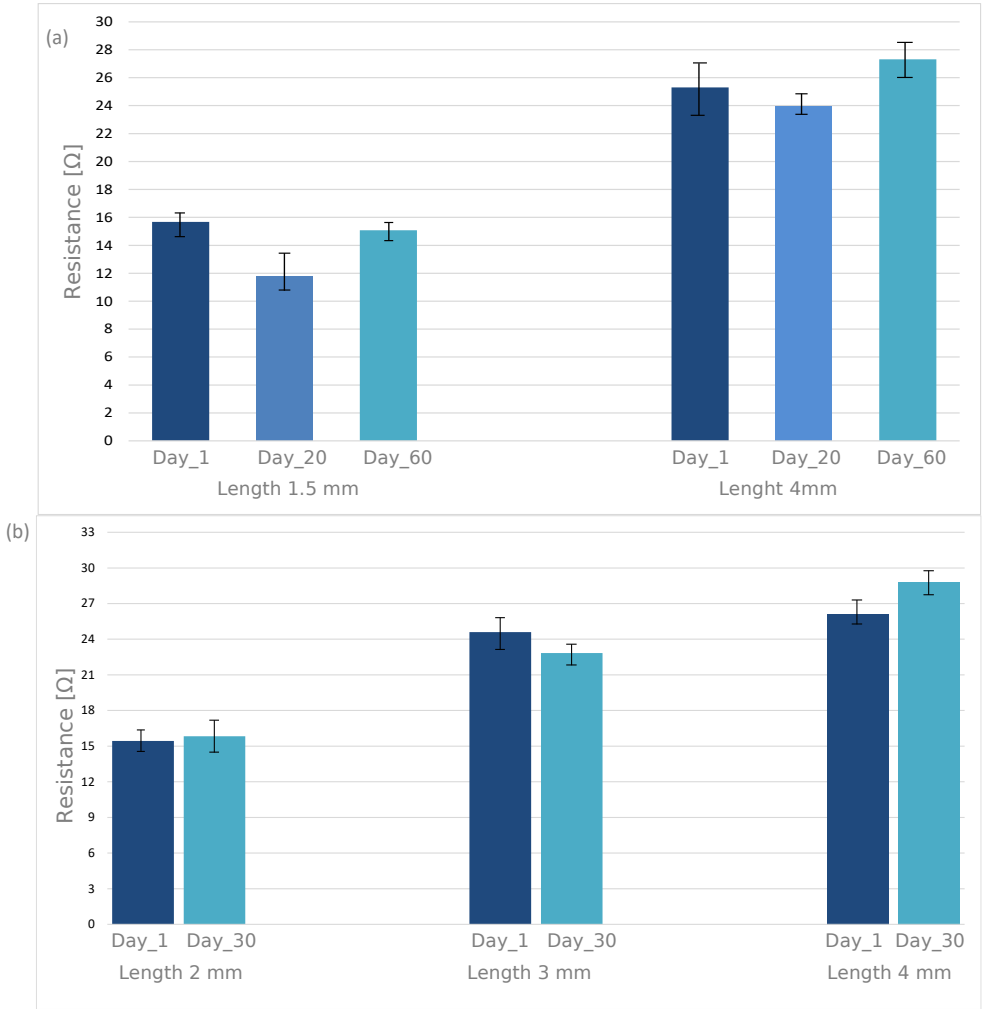

Figure 5.24: analysis of the resistance stability on different set of tracks, performed after 20 and 60 days from the first measurement (a), and after 30 days (b). Measurements done on n≥3 repetitions.

5.4 Preliminary study on ring resonators

The major problem of the embedded structures is to perform the electrical measurements with a probe-like method, where an invasive approach is involved and the setup do not assure a stable measurement. To avoid this problem we tried to think about a simple application that allows us to demonstrate the functioning of the silver structures through a wireless approach. We designed for the purpose the ring resonators to test if we are able to detect the power absorption around the resonance frequency of the resonator embedded inside the hydrogel. We tested all the resonators with different resonance frequencies, and for all the tries we obtained the same result, shown in *Figure 5.25*.

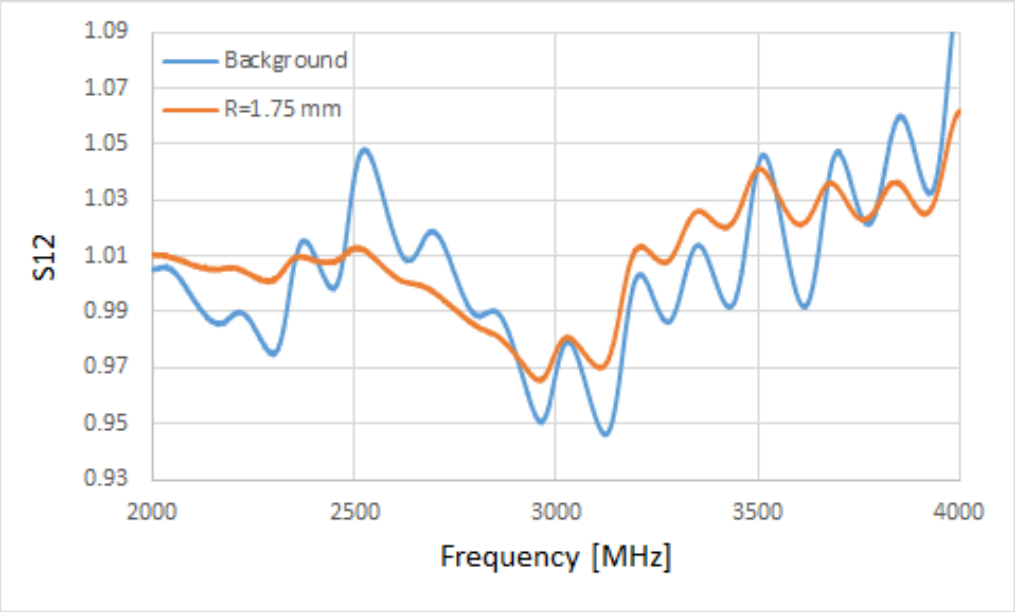

Figure 5.22: parameter S12 plotted for the background and for the resonator with radius 1.75 mm.

When testing the resonators, the hydrogel substrate placed on the transmission lines causes a huge mismatch with the reference 50 Ω load. Indeed, the presence of a material lead to a discontinuity on the line that disrupts the propagation of the electromagnetic wave. Consequently, the majority of power is lost due to reflection or absorbed by the hydrogel itself, so there is no sufficient energy arriving to the resonator that allow us to see a clear peak around the resonance frequency. Moreover, the resistivity of our structures is 3 orders of magnitude higher than the one of the bulk silver which already has a low quality factor around 10, so we expect to have a very broad peak in correspondence to the resonance frequency. This means that the absorbed power is quickly dissipated by the resonator and does not remain confined within the resonance frequency, so instead of seeing a sharp peak, we will have a smooth change in the S_{12} parameter along a larger bandwidth of frequencies. If we combine the low quality factor with the high impedance mismatch, is nearly impossible to

distinguish a resonance frequency in these conditions. We tried to measure a background signal when a piece of hydrogel without the resonator is placed on the line, to see if when the resonator is placed we could detect a significant difference in the curve that points out the presence of a peak. However when analyzing the data we obtain a curve for the resonator that follows the exact trend of the background, as we can notice the presence of the peaks along the line appearing at the same frequencies with no significant difference in the magnitude value. With the current design and equipment the quality factor and impedance mismatch seem to have a too strong influence on the quality of the results, so is not possible for now to verify the correct functioning of the device.

6. Conclusions and outlook

In this work we presented a method to achieve conductive silver structures embedded inside a hydrogel matrix using direct laser writing. The written features have a writing resolution around 20 µm and present a conductivity in the range of 10^{-6}-10^{-5} Ωm, which is three orders of magnitude higher than that of bulk silver, but is in accordance with other in-gel structures found in literature that are fabricated with analogue methods[24-25-26]. The written features have a resistance stability in time with a maximum deviation of 3 Ω obtained measuring the tracks 60 days after the first measurement, and the electrical measurements show a reliable reproducibility within the tracks of the same size, with a deviation of the measured resistance values below 10%. The advantage of using the direct laser writing technique is that we are able to obtain conductive structures directly inside the hydrogel matrix relying on the photoreduction of silver ions incorporated in the substrate. This method hence avoids further processing of the features after the writing, as there is no necessity to wash away the polymer to measure a conductivity, and it is a direct solution to obtain metallic structures embedded in a soft, biocompatible substrate without recurring to encapsulation methods. Moreover we are able to get a high spatial control of the conductive path, avoiding the detrimental effect on the mechanical properties caused by the large amount of conductive fillers that is otherwise required to obtain electrically conductive hydrogels.

6.1 Writing process limitation and improvements

The main limit for now is represented by the substrate, because we were able to achieve a conductivity of the tracks only writing inside PDMAPS hydrogels. Indeed we have to exclude the use of monomers like AMPS that have a higher swelling ratio in the PBS/glycerol solution than in the silver nitrate aqueous solution, and hydrogels that do not ensure transparency when the silver ions are incorporated in the substrate, like PAA. Even if the substrate meets these requirements, as PAM, the writing parameters require a further optimization and the writing quality will anyways strongly depend on the characteristics of the specific hydrogel. A more complete analysis on the substrate could be done by tuning the crosslinker and monomer concentration, to see if the change of stiffness has an influence on the writing quality. Indeed, it is possible that a stiffer matrix can help to give the structure more stability by holding together the silver agglomerates. The stiffness could also be used as a property to increase the diameter shrinking from silver nitrate to the PBS/glycerol solution for substrates

like PAM, where the shrinking ratio is almost null and to obtain a minimum shrink could represent a huge difference to not damage the percolation of the tracks. A key factor of the writing process is represented by the reduction of the silver ions, so we thought that increasing the molarity of the silver nitrate solution, a larger concentration of ions is present inside the matrix, and this could possibly help to increase the nucleation and growth of the particles and enhance the conductivity. A first experiment has been performed by using a 10M silver nitrate aqueous solution, and as shown in *Figure 6.1* we can notice a steeper slope in the current with respect to the tracks written with the 1M silver nitrate solution. The attempt was done measuring the conductivity on 4 different tracks of 4 mm length, and it seems that a higher conductivity is achieved by increasing the ion content in the matrix. Indeed the obtained resistance is about 16.24 Ω that is 35% lower than the analogue 4 mm tracks obtained with 1M precursor solution, and is comparable with the resistance obtained for the 2 mm long tracks. Based on this preliminary result, it would be interesting to further explore the effect of the silver ions amount on the conductivity. Anyways, increasing the amount of silver nitrate would be reasonable only if a significant increase in electrical conductivity is obtained.

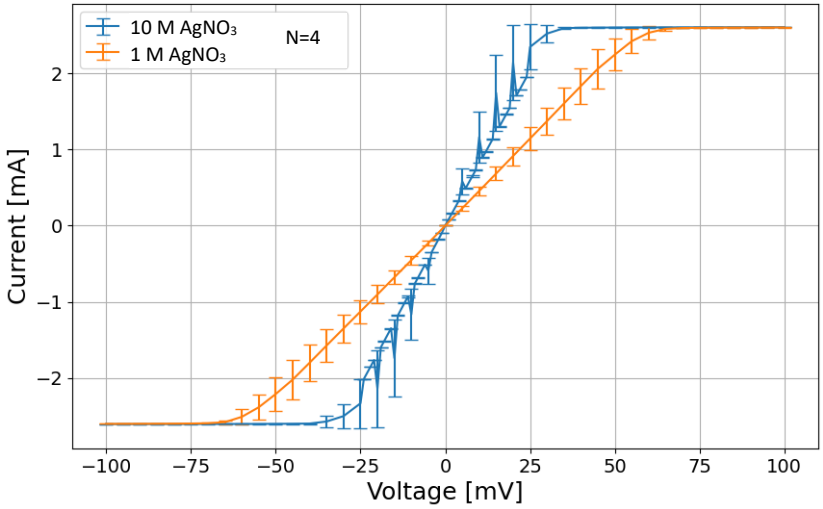

Figure 6.1: comparison between I-V curve of 4 mm tracks written using 1M and 10M silver nitrate precursor solution.

6.2 Measurement setup limits

Even if we could obtain consistent electrical results, as showed in *Figure 6.22 (b)* from the resistance/length ratio, the measuring setup still presents a strong limitation for our structures. Indeed, the position of the tips on the track influences the value of the current that depends on the quality of the contact we can achieve between the tips and the silver layer. Moreover, once we position the probes on the sample, the hydrogel can present some micro-movements due to

the matrix relaxation around the instrument or little shifts of the tips can happen due to the environment or the device itself. This causes an instability on the measured current that can slightly change the value also for measurements on the same track, and sometimes can also lead to lose the contact with the conductive layer. Hence, the electrical results are conditioned by the operator, depending on the quality of the contact that is achieved between tips and track. To facilitate this challenge a possible solution would be to increase the width of the feature to have a higher contact area, but we avoid doing this for our experiments because it considerably increases the fabrication time and the risk to have destructive bubbles during the writing. We tried to avoid this problem by designing the ring resonator and find a method to employ our conductive hydrogels in an application that can be tested wireless, but for the moment we do not obtained meaningful results. A first possible solution would be to change the resonator design to limit the problem of the low quality factor by writing bigger structures, so that we can reach lower resonance frequencies that help reduce the energy loss, and with a higher capacitance we can improve the energy storage efficiency. It would also be ideal to have a square shaped resonator as shown in *Figure 6.2,* to better match the profile of the transmission and design a costumed microstrip with a transmission line that takes into account the presence of the hydrogel and tries to compensate for the impedance mismatch with a change of the line thickness. However, the quality factor and energy loss have a quite significant influence on the measurements, so even doing such improvements on the resonators could not be enough to obtain a peak at the resonance frequency, and this could be an intrinsic limitation derived from the hydrogel and the resistivity value of the structures.

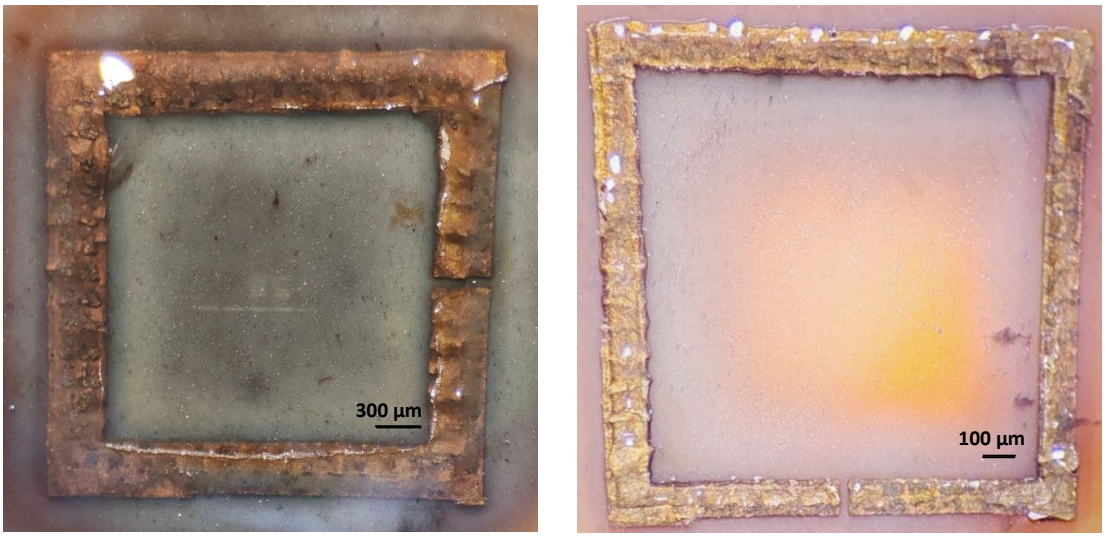

Figure 6.2: picture of the square resonators with length 4 mm and width of 500 um (a) and 300 um (b) taken with the stereomicroscope view.

7. Acknowledgements

This "chapter" is dedicated to the people who helped me to get through this Master, and shared with me all the experiences that brought me to this precise moment. No human being has been mistreated during this master. Any resemblance to real events and persons is purely coincidental.

First of all I want to thank my advisor **Professor Esther Amstad** for giving me the opportunity to collaborate with her group in these past six months, involving me in all the activities, from which I could learn a lot on soft materials and on how the world of research works. A thank goes also to my **relator Professor Matteo Cocuzza**, who sustained the writing of my thesis and answered quickly to any doubt.

A huge acknowledgment goes to the **SMaLers,** who welcomed me in the group from the first day and created the best atmosphere that made me really enjoy my time at SMaL. I could learn a lot from all of you in these months, both as scientists and as people, as each of you contribute to this little family with its special personality, and it's amazing how you can always collaborate and stimulate each other with new ideas. Thanks to my first office mates, **Antonia** in the front desk for backing me up with the office keys and the camipro and for always being a font of inspiration with her limitless knowledge; **Robin**, for being the best desk mate, always ready to cheer up the day with a joke, your imagination is a continuous stimulus for new ideas, and who knows, maybe one day I will see your face on the advertisement of your new start up and buy one of those futuristic phone chargers you want to create; uncle **Raj**, for making me taste the greatest Indian cuisine I could find in Lausanne, hope to see you on the next hike and do some other tests on the mountains' echo. A thank to the girl power of the group, **Lisa**, for supporting my bad jokes and sharing churros while watching a non-vegetarian band that is against killing cows, it always has been a good time to chat with you; **Rocio**, for being always inclusive and for being my backup in every conversation when people talk about those nerdy things we have absolutely no knowledge about; **Francesca**, for all the lunch conversations on the most disparate topics that contributed to enlarge my "cultura generale" and for being the defense ambassador of Italian culture; **Tyaniu**, for bringing joy in the lab with your spirit and for being the best food advisor for dinners at Kung-Fu; **Eva** for being this tireless burst of energy in every situation, always ready to keep the morale high with some anecdote, thanks for sharing the oven during your

polymerizations; **Alex**, for sharing the most focused days in the last weeks of my thesis, your determination and organization have been inspiring for me; **Allison**, it's been a short period together but the few moments we shared I could appreciate your kind and joyful spirit; **Ran**, my first PhD defense, for eating bao buns together and sharing some great conversations in the few weeks we met; **Pauline** for the tasty snacks you brought back from Japan; **Gaia** for making me one of her last amazing birthday cakes. To finish off, a thank goes also to the male representatives **Zoubeir**, the greatest game nights organizer, for sharing the ways back to Renens in the metro, and all the Thai food advices (looking forward to try the carbonara); **Brian**, for the efforts in giving an insight on the U.S. culture and the limitless elucidations on the American measurement system. I wish you all the best for your future, you have been an amazing group!

A special thank goes to **Lorenzo**, it has been a real luck for me to have you as supervisor during these six months. With your patience and passion you transmitted me the knowledge and interest that I needed to make this project not just a thesis, but my first little research to put all myself into. You were able to make me affectionate to the project and to teach me how to do research, by making me feel part of a team and not just a student following the supervisor directives. This great atmosphere of collaboration you created, allowed me to propose my ideas and gave me the independence I needed to be satisfied of myself and of what I could achieve with my abilities. I couldn't be happier of what I learned working with you, both as scientist and person. I wish you all the best for your future, whether it will see you on the cover of Nature for a breakthrough in the hydrogel conductivity, or on the Rolling Stones magazine as the new music legend who climbed the Spotify rankings of the year. However it goes, keep enjoying life with a smile, limitless kindness and a bit of good Italian sarcasm…and of course music and homemade pizza! Thank you again for everything you have done for me, I really enjoyed working with you in these months. I will keep in touch to know the new progresses of the project, and the dates of the next concerts. Good luck for everything!

From the laboratory, I drive back to home, where I have to acknowledge all the members of my family that have been of great support, not only in the last two years but through every little step of my life. Ringrazio **mamma** e **papà** per tutte le opportunità che mi avete dato di imparare, sia di scienza che sulla vita. Mi avete sempre supportato in tutte le mie scelte, anche le meno ordiniarie, dandomi sempre la sicurezza di avere un appoggio a sostenermi nel caso fossi caduta. Tutto quello che ho raggiunto è anche merito vostro e sono felice di avervi vicino, ovunque io sia. Grazie a mia sorella **Giulia**, che è sempre stata un riferimento per

me, il posto sicuro in cui so di poter tornare in qualsiasi momento. Anche a distanza mi sei sempre stata vicina, che fosse con un messaggio, una fotografia o un reel su instagram senza risposta, ogni giorno sei stata presente facendomi sentire a casa con voi. La connessione che c'è tra di noi, ogni volta che pensiamo la stessa cosa, quando basta uno sguardo per capirci, mi fa realizzare che dono sia avere una sorella e quanto tu sia insostituibile. Un grazie a **Luci**, che da quando sono piccola si è sempre presa cura di me, con una pazienza e un affetto sconfinati. Mi hai aiutata a sopravvivere da studente fuorisede grazie ai tuoi insegnamenti culinari, sempre pronta a venirmi in soccorso quando mi serviva l'ennesima ricetta di quel piatto che mi cucinavi sempre, quando avevo bisogno di senitrmi a casa. A **Sara** che ha sempre creduto in me ed è sempre stata fiera delle mie scelte, prima ancora che lo fossi io. Grazie a te e **Barros** per avere sempre un pensiero per me, anche quando le occasioni di vedersi sono poche. Un grazie a **Anna** che si preoccupa sempre per me, e non perde mai l'occasione per mandarmi un rifornimento di cibo appena torno a casa. A **nonna**, per tutte le telefonate per controllare che fossi ancora viva. Grazie a te e a **nonno** per esservi presi cura di me quando ero piccola, per i pranzi della domenica e le estati insieme al mare, che hanno contribuito a creare dei bei ricordi di casa.

And to end this chapter, from the blood family to the adopted family of all my friends who has been with me in all those years of being a student. Starting from the beginning of the story I want to thank **Virginia** and **Eleonora**, with whom I shared the craziest adventures of my youth. Despite our lives followed different paths, after more than ten years I can still find a support in you and when I come back home you are always on the list of few people I want to spend my little time with and find back the comfort of the old times. A thank to **Flou**, for keep being my captain also outside of the field, checking on me and keeping the morale high; always ready to welcome me back home with a ritual beer and pizza night. Coming to the most recent days, a thank goes to the Nanotech team for sharing this troubled journey together. In particular I want to thank "The boys", **Cyprian** and **Ewan**, for sharing the climbing and ski sessions, and all the disgusting lunches at the French canteen. **Marius** for being the most loyal…and only Svizzero in the course and for always taking care of "The girls". You always kept our attention level high with all your attempts to kill us on the mountains, even if in the end it was worth it. To **France**, the best and iconic neighbor one could ask for in Vennes. Thanks for being our adopted sciura, sharing the infinite study sessions in interlingua and for the talks at midnight on the metro, about the differences between Ascension and Assumption of the Virgin Mary. A thank goes also to **Julian**, my project mate in the beginning of this adventure. Thank you for

saving me from sleeping under a bridge, even when we had known each other for not that long.
Last, but surely not least, I want to thank the true highlight of the Master, the friends without whom I might not have survived this journey with no evident damage. You made every day to feel lighter, distracting me from the stress of the exams, and the bond that grew in these two years between us, was able to fill the void left by being far from home. Together we shared every single day, we laughed, we cried, and in you I found a second family, with whom I could really be myself. Thank to **Chiara** for keeping me updated on the news from the French border, and for the supply of taralli pugliesi doc that supported my aperò after work. You enlightened the sad university days with your impeccable style, you kept my sugar level high with your professional cakes and you kept the spirits high with a right dose of healthy madness and drama. You will remain the favorite guest of my one-meter bed in Vennes and of course of my red pigiamino. To **Geppi**, for singing with me the revival hits of 2010 in the kitchen at night, with a half can of beer in the body and the greatest disco lamp on the market. You have been my Alicia when No One was mad enough to follow me, restless worker at day and greatest entertainer at night. For sure your paparazzi pictures will always be an unforgettable memory in my phone gallery. To **Cia**, thanks for being my next-door roommate in every house we switched during the Master, I remember every knock on the wall at 1 a.m. before going to sleep. We can be the craziest duo if we are on a good day, going from Dos Oruguitas to several attempts of suffocation with the pillows, but in the end I always tuck you in. I will keep crossing Europe to see you, what other vegan person would host your meat in her freezer when you have no space. Thank to **Vale**, mum, nicknames supplier, study and cooking mate. We basically lived the last two years in symbiosis, making the same bad decisions but always coming out from them together, more or less successfully. With you and parrot I shared the best trips back to Italy, together we faced the worst study sessions from Comala, to Berlioz, to Rolex, and went through all the Swiss hikes and exciting parties of Saint-Genis. We never spent more than two weeks without seeing each other, and despite of this I am still not tired of you. I hope to continue this short distance friendship, and keep watching our favorite trash movies together on Friday nights.

8. References

1. LEONARDO DA VINCI. *Leonardo da Vinci* https://www.leonardodavinci-italy.com/it/volo.
2. Yuk, H., Wu, J. & Zhao, X. Hydrogel interfaces for merging humans and machines. *Nature Reviews Materials* **7**, 935–952 (2022).
3. Tran, V. T., Mredha, Md. T. I. & Jeon, I. High-water-content hydrogels exhibiting superior stiffness, strength, and toughness. *Extreme Mechanics Letters* **37**, 100691 (2020).
4. Kougkolos, G., Golzio, M., Laudebat, L., Valdez-Nava, Z. & Flahaut, E. Hydrogels with electrically conductive nanomaterials for biomedical applications. *Journal of Materials Chemistry B* **11**, 2036–2062 (2023).
5. Yuk, H., Lu, B. & Zhao, X. Hydrogel bioelectronics. *Chemical Society Reviews* **48**, 1642–1667 (2019).
6. Mehta, P., Sharma, M. & Devi, M. Hydrogels: An overview of its classifications, properties, and applications. *Journal of the Mechanical Behavior of Biomedical Materials* **147**, 106145 (2023).
7. Hu, W., Wang, Z., Xiao, Y., Zhang, S. & Wang, J. Advances in crosslinking strategies of biomedical hydrogels. *Biomaterials Science* **7**, 843–855 (2019).
8. Bashir, S. *et al.* Fundamental Concepts of Hydrogels: Synthesis, Properties, and Their Applications. *Polymers (Basel)* **12**, 2702 (2020).

9. Guimarães, C. F., Gasperini, L., Marques, A. P. & Reis, R. L. The stiffness of living tissues and its implications for tissue engineering. *Nat Rev Mater* **5**, 351–370 (2020).

10. Feig, V. R. *et al.* Conducting polymer-based granular hydrogels for injectable 3D cell scaffolds. *Adv Mater Technol* **6**, 2100162 (2021).

11. Liu, Y. *et al.* Soft and elastic hydrogel-based microelectronics for localized low-voltage neuromodulation. *Nat Biomed Eng* **3**, 58–68 (2019).

12. Sagdic, K., Fernández-Lavado, E., Mariello, M., Akouissi, O. & Lacour, S. P. Hydrogels and conductive hydrogels for implantable bioelectronics. *MRS Bulletin* **48**, 495–505 (2023).

13. Tabrizi, S., Cao, Y., Lin, H. & Jia, B. Two-photon reduction: a cost-effective method for fabrication of functional metallic nanostructures. *Sci. China Phys. Mech. Astron.* **60**, 034201 (2017).

14. Thanh, N. T. K., Maclean, N. & Mahiddine, S. Mechanisms of Nucleation and Growth of Nanoparticles in Solution. *Chem. Rev.* **114**, 7610–7630 (2014).

15. Ostwald ripening. *Wikipedia* (2024).

16. Tanaka, T., Ishikawa, A. & Kawata, S. Two-photon-induced reduction of metal ions for fabricating three-dimensional electrically conductive metallic microstructure. *Applied Physics Letters* **88**, 081107 (2006).

17. Maruo, S. & Fourkas, J. t. Recent progress in multiphoton microfabrication. *Laser & Photonics Reviews* **2**, 100–111 (2008).

18. Waller, E. H. & Freymann, G. von. From photoinduced electron transfer to 3D metal microstructures via direct laser writing. *Nanophotonics* **7**, 1259–1277 (2018).

19. Tensile Testing: Machine and Tester. *Tensile Testing: Machine and Tester* https://www.zwickroell.com/products/static-materials-testing-machines/universal-testing-machines-for-static-applications/tensile-tester/.

20. Nanoscribe Photonic Professional GT+. *EPFL* https://www.epfl.ch/research/facilities/cmi/equipment/photolithography/nanoscribe-photonic-professional-gt/.

21. Pinheiro, T. *et al.* Direct Laser Writing: From Materials Synthesis and Conversion to Electronic Device Processing. *Advanced Materials* **n/a**, 2402014.

22. Waller, E. H., Duran, S. & Von Freymann, G. Direct laser writing of 3D metallic mid- and far-infrared wave components. *Nanophotonics* **12**, 1549–1555 (2023).

23. info. Bulk Resistivity and Conductivity of Metals. *Deringer Ney* https://deringerney.com/bulk-resistivity-and-conductivity-of-metals/ (2022).

24. Stellacci, F. *et al.* Laser and Electron-Beam Induced Growth of Nanoparticles for 2D and 3D Metal Patterning. *Advanced Materials* **14**, 194–198 (2002).

25. Komori, T., Furukawa, T., Iijima, M. & Maruo, S. Multi-scale laser direct writing of conductive metal microstructures using a 405-nm blue laser. *Opt. Express, OE* **28**, 8363–8370 (2020).

26. Waller, E. H., Karst, J. & Freymann, G. von. Photosensitive Material Enabling Direct Fabrication of Filigree 3D Silver Microstructures via Laser-Induced Photoreduction. *gxjzz* **2**, 228–233 (2021).

27. du Plessis, A., Broeckhoven, C., Guelpa, A. & le Roux, S. G. Laboratory x-ray micro-computed tomography: a user guideline for biological samples. *GigaScience* **6**, gix027 (2017).

28. Keklikoglou, K. *et al.* Micro-computed tomography for natural history specimens: a handbook of best practice protocols. *European Journal of Taxonomy* (2019) doi:10.5852/ejt.2019.522.

29. Dautta, M. *et al.* Multi-Functional Hydrogel-Interlayer RF/NFC Resonators as a Versatile Platform for Passive and Wireless Biosensing. *Advanced Electronic Materials* **6**, 1901311 (2020).

30. 4D printing of Metal-Reinforced double network granular hydrogels - ScienceDirect. https://www.sciencedirect.com/science/article/pii/S1385894723041645.